Universitat Autònoma de Barcelona

Link between microstructure and properties in new metallurgical concepts for very low loss non-oriented electrical steel

Name: Ana Rodríguez Alonso

UAB director: Mº Dolors Baró

Company director: Daniel Ruiz Romera

Date: 19/09/2008

OCAS NV
John Kennedylaan 3
B-9060 Zelzate
Tel : +32 9 345.12.11
Fax: +32 9 345.12.04
www.ocas.be

Zelzate, 10 February 2009

CERTIFICATION FOR PROJECT PRESENTATION AND DEFENCE

Ana Rodriguez Alonso has been working in OCAS on the project “Link between microstructure and properties in new metallurgical concepts for very low loss non-oriented electrical steel.”
She was closely followed-up and supervised, and meetings on a regular basis showed that she was progressing very well with this project.

I consider that Ana is suitable and well prepared, and I hereby authorize her presentation and the subsequent defence.

Daniel Ruiz Romera
Research Engineer

OCAS NV OnderzoeksCentrum voor Aanwending van Staal (Research Centre for the Application of Steel)
Registered Office: John Kennedylaan 3, B-9060 Zelzate, Belgium - VAT BE 0444 177 945 - Trade Register Gent 161 759
Bank Account (Fortis) 290-0030977-55 – IBAN BE 31 2900 0309 7755 – BIC GEBABEBB

Table of Contents

Problem description **4**
1 Introduction **5**
1.1 Soft Magnetic Materials 5
1.1.1 Types of Soft Magnetic Materials 5
1.1.2 Magnetization and domain structure 6
1.1.3 Energy losses 7
1.2 Electrical steels 8
2 Methodology **9**
2.1 Flow chart 9
2.1.1 Influence of Mn, Ni and Cr on low loss electrical steels 9
2.1.2 Effect of soaking temperature on the magnetic properties and grain size of electrical steels with different chemistries 10
2.2 Sample preparation for metallography 10
2.2.1 Cutting 10
2.2.2 Embedding 11
2.2.3 Grinding 11
2.2.4 Polishing 11
2.2.5 Etching 11
2.3 Optical microscope observation 12
2.4 Grain size measurement 12
2.4.1 Intercept procedure 12
2.5 Electron microscope observation 13
2.5.1 Gold layer deposition 14
2.6 Sample preparation for texture 14
2.6.1 Cutting 14
2.6.2 Embedding 15
2.6.3 Grinding and polishing 15
2.7 Texture measurements 15
2.7.1 Overview of texture analysis 15
2.8 Texture measurements 18
2.9 Gleeble tests 19
2.10 Magnetic measurements 20
2.10.1 Loss separation 20
3 Materials **21**
3.1 Influence of Mn, Ni and Cr on low loss electrical steel 21
3.1.1 Effect of soaking temperature on the magnetic properties and grain size of electrical steels with different chemistries 21
4 Results **23**
4.1 Influence of Mn, Ni and Cr on low loss electrical steel 23
4.1.1 Introduction 23
4.1.2 Laboratory casting 23
4.1.3 Laboratory processing 24
4.1.4 Magnetic properties 25
4.1.5 Microstructural analysis 28
4.1.6 Texture 31
4.1.7 Results correlations 34
4.2 Effect of soaking temperature on the magnetic properties and grain size of electrical steels with different chemistries 35
4.2.1 Introduction 35
4.2.2 Magnetic properties 38
4.2.3 Grain size 39
4.2.4 Correlation between P15 and grain size 42
4.2.5 Oxidation 42
5 Conclusions **50**

5.1 Influence of Mn, Ni and Cr on a low loss electrical steel....50
5.2 Effect of soaking temperature on the magnetic properties and grain size of electrical steels with different chemistries....50
6 Bibliographic references....52
7 Appendix....54
7.1 Measured data for Mn, Ni and Cr addition samples....54
7.2 Experimental Gleeble test....55
7.3 Data obtained after Gleeble tests....66
8 Summary....74

Problem description

Nowadays, the energy efficiency of electrical devices is crucial for the environmental protection. To improve the energy efficiency it is critical to reduce the core loss of these devices. The development of new steel grades with lower magnetic losses is one of the goals of ArcelorMittal.

The steel losses depend essentially on the composition, microstructure, crystallographic texture and processing parameters. It is interesting to optimize both the chemical composition and the processing parameters in order to have the best magnetic performance.

The aim of this study is twofold.

- Literature shows contradictory results about the influence of some alloying elements on the magnetic loss of very low loss non oriented electrical steels. This is the case of Mn, Ni and Cr. This study aims to understand the effect of these elements on the microstructure, texture and properties of electrical steels in order to try to introduce some new alloying concepts for electrical steels

- A crucial processing step is the final annealing, i.e. the chosen temperature (soaking temperature) and time. They will determine the final grain size, which is a crucial parameter for the behaviour of the magnetic losses. The study also aims to understand the influence of the annealing temperature on the grain size for different alloying contents and to find what is the optimum grain size for every chemical composition

1 Introduction

1.1 Soft Magnetic Materials

One of the main goals of our society is to generate, transmit and transform electrical energy with the minimum losses. In these processes are involved apparatus such as generators transformers and electrical motors which cores are made of the so-called soft magnetic materials. These ferromagnetic materials are characterized by their high permeability and low coercivity, which turns into high values of induction when a low field is applied and low core losses.
Another important property of the soft magnetic materials is their high value of the electrical resistivity, since it decreases the energy losses due to Eddy currents. They are electrical currents that appear when an alternating field is applied, and are one of the main sources of energy losses.

1.1.1 Types of Soft Magnetic Materials

Soft magnetic materials can be classified in four different groups [1]: 1) metallic materials 2) ferrites and compounds, 3) amorphous and nanocrystalline materials and 4) thin films.

Metallic materials are normally used in d.c. and a.c. apparatus at frequencies below 1kHz. Among the metallic materials the most important are Fe-Si and Fe-Ni alloys. Fe-Si alloys, usually known as *electrical steels*, are the most important soft magnetic materials in production and economic volume. They are mainly used in power generation and transformation. Fe-Ni alloys or permalloys are very versatile. The main uses of these alloys are the inductance coils and transformers working at audio and at very high frequencies. They can be made with low or zero magnetostriction and they have high permeabilities and low coercitivities.

Amorphous materials are produced by rapid quenching of magnetic alloys consisting of Fe, Ni and/or Co and more than one of the following elements: boron, silicon, phosphorus or carbon. As a result of the rapid cooling these materials do not form a crystalline state. They have very low coercitivity and high permeability although the saturation induction can be very low. Their main applications are: sensors, magnetostrictive transductor and pulsed power transformers.

Nano-crystalline materials, which are produced by annealing the amorphous material, have been more recently investigated. These alloys can be single phase but usually comprise nano-sized grains, in the range 10-50 nm. They have a resistivity, a low anisotropy and a good mechanical strength.

Ferrites are used at frequencies above 1kHz and in computer memory cores. There are several types of ferrites which are used depending on working frequency.

1.1.2 Magnetization and domain structure

To evaluate the behavior of a ferromagnetic material in a magnetic field is practical to plot the magnetization M or the induction B against the magnetic field H. Fig.1 shows a typical magnetization curve of a ferromagnetic material when an alternating field is applied, the so-called hysteresis loop. When a ferromagnetic material is magnetized in one direction, there is a remaining magnetization that does not disappear when the imposed magnetic field is removed. Actually it is necessary to apply a field on the opposite direction to the initial one to remove the remaining magnetization, this field is known as coercitive field, Hr. To characterize the hysteresis loop there are other parameters that are useful: remanence Mr is the magnetization that remains when the field is removed, M_s (saturation magnetization) is the highest value of the magnetization and μ is the permeability that is defined as the slope of the curve.

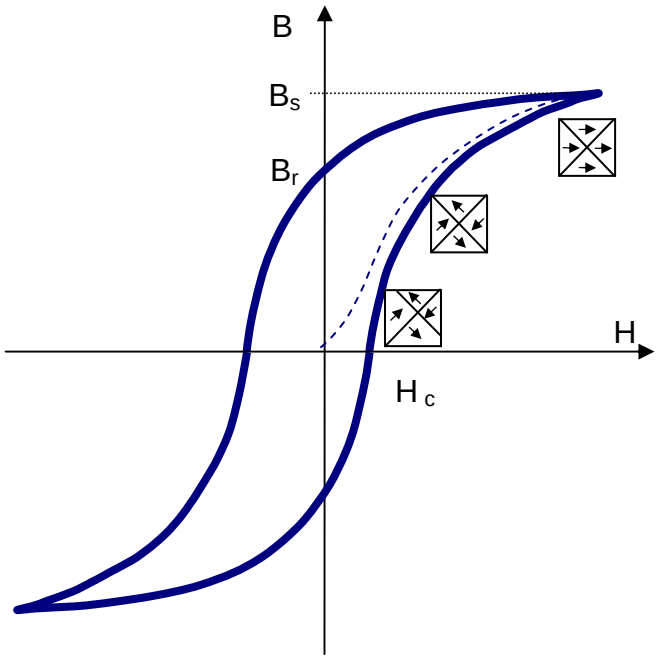

Figure 1 *Hysteresis loop of ferroelectric material*

The hysteresis loop can be explained by the introduction of magnetic domain theory. Ferromagnetic materials are made up of small regions known as magnetic domains. In each domain, all of the atomic dipoles are coupled together in a preferential direction. When the material is unmagnetized the direction varies from domain to domain, so all available preferential directions will be used equally in the material. Hence the specimen as a whole will not show a net magnetization. When a magnetic field is applied, the domains change shape and size by the movement of domain boundaries, the domains that are oriented in directions nearly aligned with the applied field grow at the expense of those that are unfavourably oriented. This process continues with increasing field strength until the

specimen becomes a single domain, which is nearly aligned with the field. The saturation is achieved when this domain, by means of rotation, becomes oriented parallel to the magnetic field H.
When the magnetic field is removed in spite of some of the domains loss the alignment there is a fraction that remains aligned producing a remanent magnetization M_r, to demagnetize the material is necessary to apply an external field (H_c) in the direction opposite to that of the original field.

1.1.3 Energy losses

Due to the irreversibility of the magnetization and demagnetization process, there is an amount of energy that is loss during the process. It can be computed as the a area inside the hysteresis loop and is given by

$$P_{tot} = \oint BdH \qquad (1)$$

This energy is converted to heat and dissipated into the lattice. This effect is undesirable in the case of soft magnetic material, not only because of the waste of energy, but also for the consequences of heating the material.
The area of the hysteresis loop depends on the frequency of the alternating field applied. To compute static contributions it can be defined the hysteresis losses P_h as the area of the hysteresis loop when a quasi-static field (0.1 Hz) is applied.
Another source of losses are the Eddy currents. When the field is applied on the specimen appears an electromotive force (emf) on the body. If the material is good conductor then an appreciable amount of electrical currents emerge producing an increase of the energy loss, P_F, through joule heating (Foucault losses).

Experimental measurements indicate that the total energy (area of the hysteresis loop) is larger than the sum of hysteresis losses and eddy current losses.

$$P_{tot} \geq P_F + P_h \qquad (2)$$

The discrepancy between them is known as anomalous or excess losses:

$$P_e = P_{tot} - P_F - P_h \qquad (3).$$

1.2 Electrical steels

Steels for electrical use or electrical steels are of great importance for industry worldwide, since they are used in electrical engines and transformers which energy efficiency depends on the magnetic permeability and magnetic losses associated with alternating current excitation. They are primarily silicon-iron alloys, with a silicon concentration from zero to 6.5%. Thanks to the Si addition eddy current losses can be reduced [4], but there are important drawbacks to this method: First the magnetic flux density declines and second, the hardness and brittleness increase which adversely affects the workability of the material. However, magnetic properties not only depend on the silicon composition but also in other properties such as chemical composition, process variables, precipitates, microstructure, and texture [6, 9, 10, 11, 13].

Electrical steels can be divided in two groups: Grain oriented electrical steels (GO) and non-oriented (NO). GO steels are grain-oriented in a specific direction consisting mainly of Goss orientation of (110)[001] which is favourable to magnetic properties of induction and core loss, and are thus used mainly for transformer cores. Manufacture of GO steels consists of complicated processes and there are many difficulties associated with controlling Goss orientation. In contrast, NO steels do not require a unidirectional orientation because they are used for electrical rotatory devices such as motor cores. The control of unidirectional oriented-grains is not necessary for NO steels, and thus the manufacturing processes of NO steels are comparatively simple and economical.

2 Methodology

2.1 Flow chart

The following flow charts present the experimental procedure followed in this investigation. In blue are showed the processing steps, in green the sample preparation and in yellow the different characterization techniques.

2.1.1 Influence of Mn, Ni and Cr on low loss electrical steels

The microstructure after each important step of the processing (Hot rolling, hot band annealing and continuous annealing) has been analyzed. Moreover, the magnetic properties, grain size and crystallographic texture after the final annealing step have been also studied

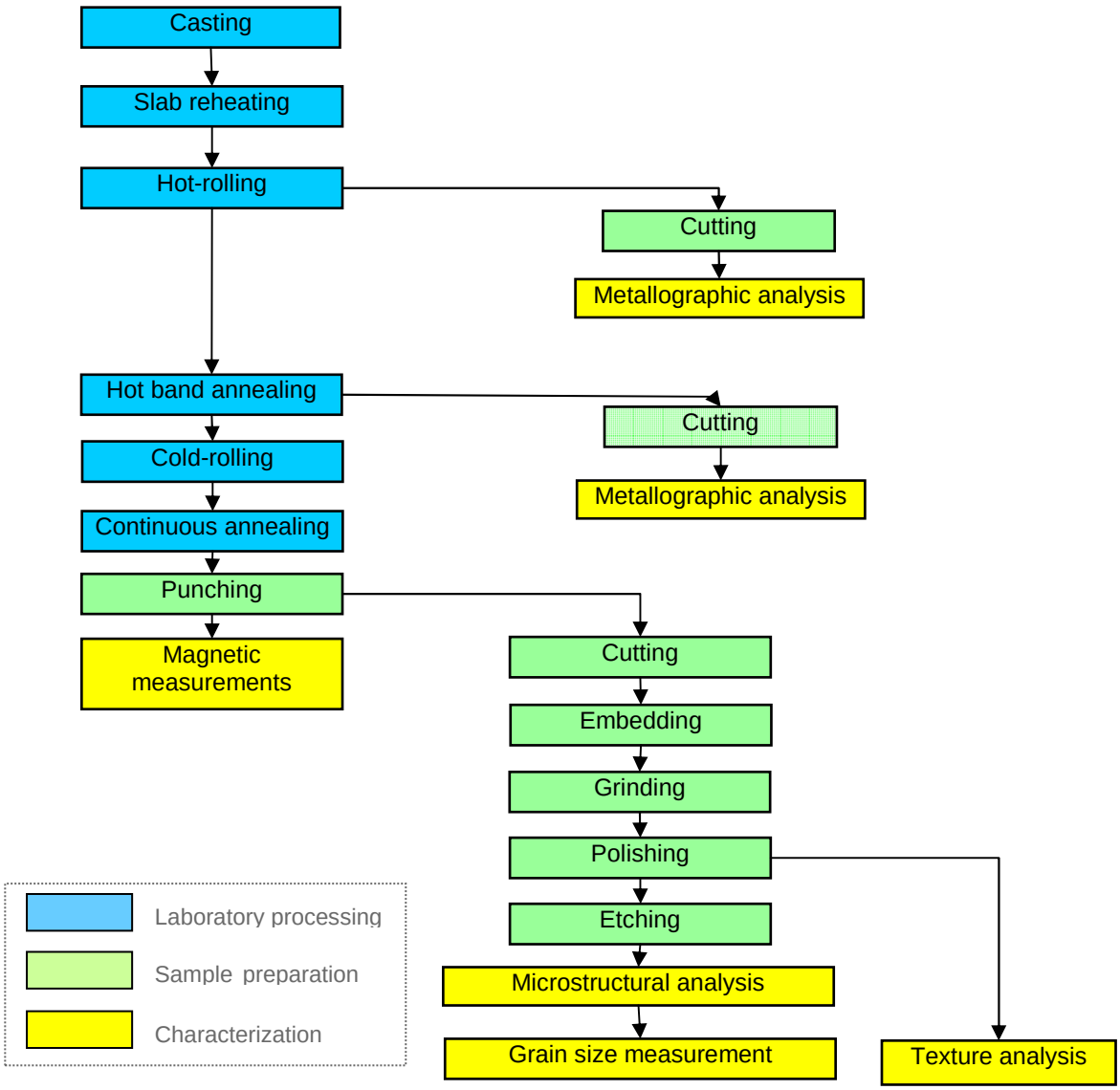

2.1.2 Effect of soaking temperature on the magnetic properties and grain size of electrical steels with different chemistries

By means of the Gleeble 1500 D simulations of the final annealing step have been performed. Afterwards the magnetic properties, grain size and surface oxidation have been analyzed.

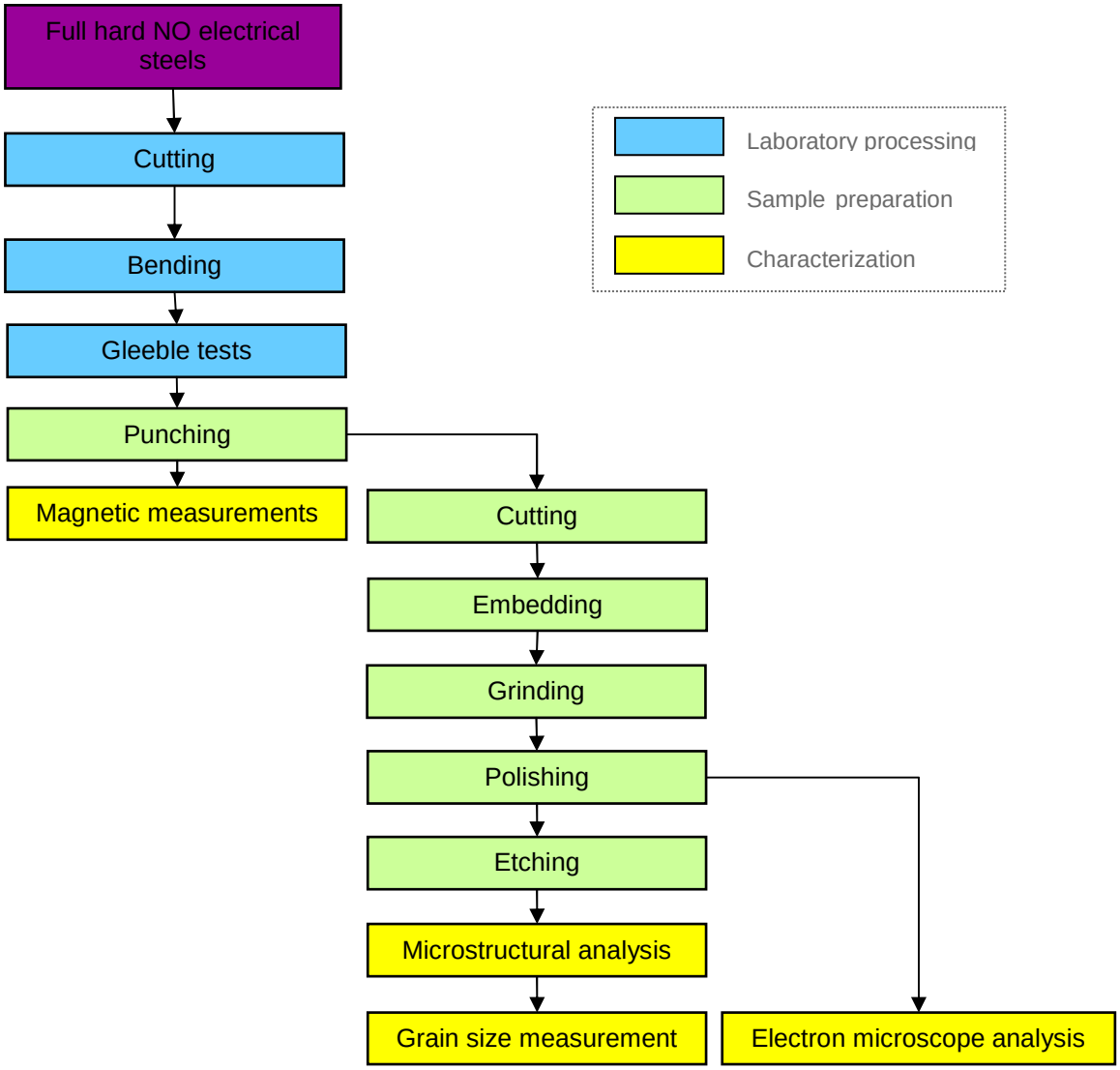

2.2 Sample preparation for metallography

2.2.1 Cutting

The samples were cut to observe their cross section in the rolling direction Due to the restricted dimensions of the embedding machine the size of the samples is approximately 20x10 mm, where 20 mm are in the rolling direction, and 10 mm in the normal direction. Depending on the thickness of the samples they can be cut in two different cutting machines. In the case of samples of a thickness less

than 1,5 mm it is used a guillotine (De Tollenaere model GG-49, Gerver Walker) and in the other cases it is used Discotom 5 Struers cutting device.

2.2.2 Embedding

To embed the samples it is used the machine ProntoPress-10, Struers. When the samples are thicker than 0.5 mm they are embedded using two resins: first durofast and after multifast, and a pre-setup method named durofast. To embed with these resins it is necessary to apply high temperatures, so in the case of thinner samples, to avoid bending, a molded durofast resin was use in order to have finest grains. It was also used a special method that consist in:

- *Preheating:* t=3min, T=160ºC, F=0N
- *Heating*: t=5min, T=180ºC, F=20KN
- *Cooling:* Cooling rate=High, t=3min

2.2.3 Grinding

To remove the material close to the cutting border it is necessary to grind the sample. It is used two grinding plates: 80 and 220 (number of SiC grains by square inch), approximately 3 min each one, a force of 35N and a speed of 300 rpm. During the grinding process the sample is lubricated with water. Between each step the sample is cleaned with water and dried with air compressed. The sample holder is also cleaned.

2.2.4 Polishing

The samples are mirror like polished in three steps using MD/DP Largo, Dac and Nap Struers plates, and a water-based solution of diamond particles suspension with sizes 9,3,1 μm respectively. It is polished during 3 min and a force of 35N in Largo and Dac plates, and 1.5 minutes and a force of 25N in Nap step. The speed is 150 rpm and it is lubricated with DP-lubricant.
Between each step, the samples are cleaned with methanol, dried with air compressed and finally softly cleaned with acetone. The sample holder is also cleaned.

2.2.5 Etching

To observe the microstructure of the sample, it is etched with Nital 2% or 4% (solution of HNO_3 and ethanol). The time of the attack and the concentration of the solution depend on the sample. Normally, when it is microstructure after hot rolling it is better to use Nital 4% and when it is microstructure after continuous annealing it is better Nital 2%. It is important to etch it just after polishing to avoid oxidation.
After etching it is cleaned with methanol, dried with compressed air and cleaned softly with acetone.

2.3 Optical microscope observation

The microscope used is Axiovert 200M. It has been observed three kinds of microstructure: After hot rolling, after band annealing and after continuous annealing. In the case of grain size measurement it is useful to use the filter that highlights the grain boundaries.

2.4 Grain size measurement

The grain size measurement has been done following the intercept procedure of the ASTM 112-96 standard.

2.4.1 Intercept procedure

The intercept procedure consists in measuring the number of grains intercepted by a test line or the number of grain boundary intersection with a test line, per unit length of test line. The method of counting the grain intercepts and the grain boundary intersections are equivalent; in this work only the ***grain boundary intersections*** are counted (see Fig.2). The grain boundary intersection count is the determination of the number of times a test line cuts across, or is tangent to, grain boundaries (triple point intersections are considered as 1-1/2 intersections). Therefore, the grain boundary intersection per unit length is computed as:

$$N_L = \frac{\bar{I}}{L} \qquad (4)$$

Where L is the length of the test line and $\bar{I}$ the mean number of grain boundary intersections.
Four test lines have been taken, as is shown in Fig. 2, hence *L* is computed as the sum of the length of the four test lines:

$$L = H + V + D1 + D2 \quad (5)$$

The number of intersections must be at least 250, therefore, it 5 photographs of each sample have been taken. $\bar{I}$ can be calculated as

$$\bar{I} = \frac{\sum_{n=1}^{5} I_n}{5} \qquad (6)$$

Where I_n is the number of grain boundary intersections for each image.

The ASTM grain size, G, was originally defined as:

$$N_{AE} = 2^{G-1} \qquad (7)$$

Where N_{AE} is the number of grains per square inch at 100X magnification.

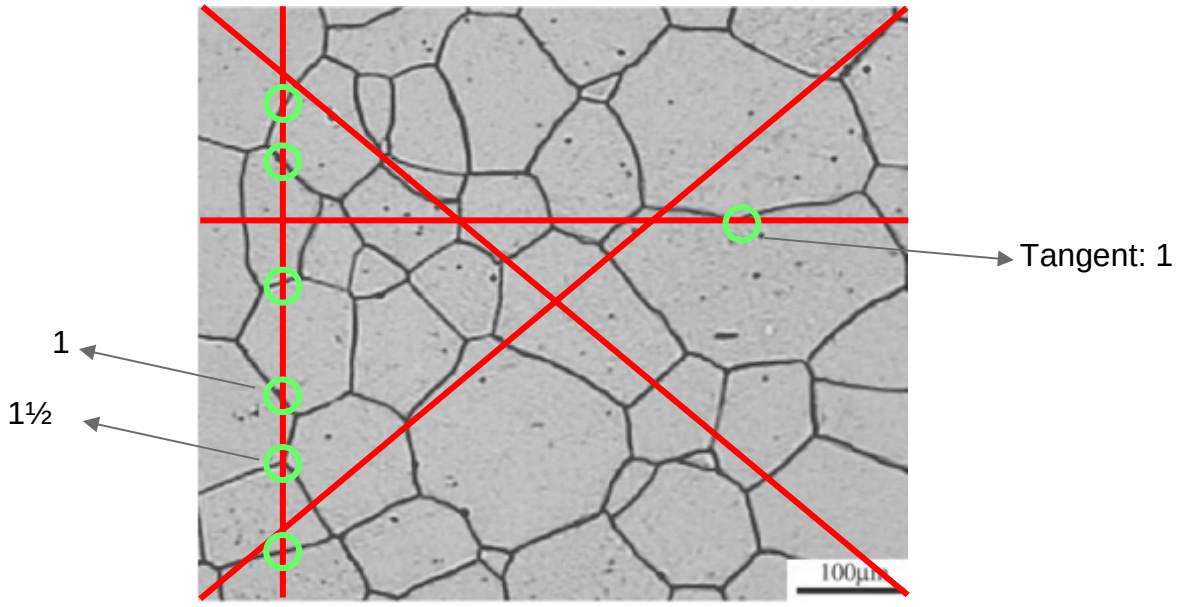

Figure 2 *Grain boundary intersections method*

The relation between the ASTM grain size, G, and the mean lineal intercept procedure is given by

$$G = -3.2877 + 6.643856 \cdot \log10(N_L) \quad (8)$$

By means of the ASTM grain size can be calculated the mean diameter as:

$$D_M = 359.08 \cdot \exp(-0.3464G) \quad (9)$$

2.5 Electron microscope observation

To observe the oxidation of the samples two different electron microscopes have been used: the LEO 15-30 Scanning Electron Microscope (SEM) and the JXA-8800L Jeol Electron Probe Microanalyzer (EPMA). The main difference between them is that with the first one it is possible to achieve magnification of 5.10^5X, while in EPMA is only possible 2.10^4X; the other difference is that in the case of EPMA it is also possible to do backscattered electron microscopy. Both microscopes have a XRD device that permits to obtain the XR spectrum and to perform XRD mappings.

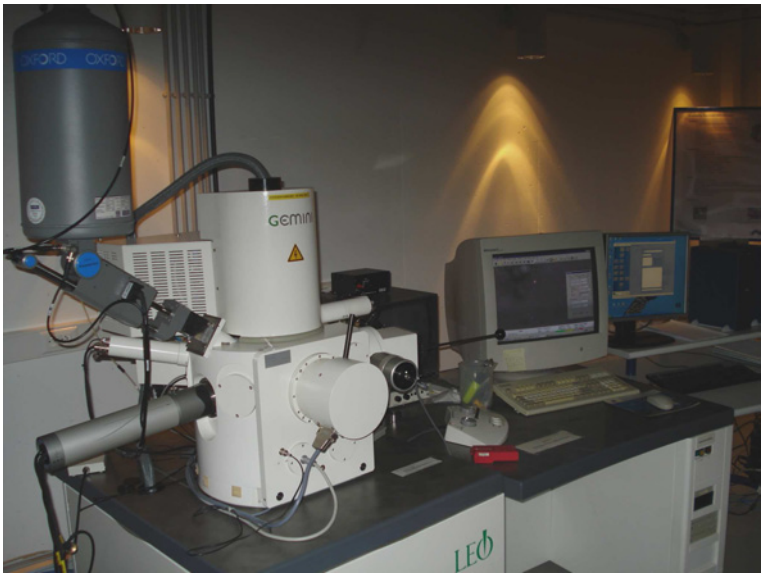

Figure 3 *SEM LEO 15-30*

2.5.1 Gold layer deposition

To observe the samples in the electron microscopes, by means of the BALZER SCD050 sputter coater a gold layer is deposited over the bakelite to make it more conductive. Afterwards, the sample is connected with the sample holder of the electron microscope using a carbon tape (see Fig.4) in order to conduct the electrons out of the sample

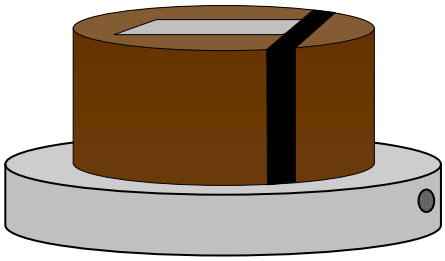

Figure 4 *Carbon tape*

2.6 Sample preparation for texture

2.6.1 Cutting

To measure texture it is interesting to observe the rolling plane, therefore, in this case the samples are cut with a size of 15x20 mm where 15 mm is the transversal direction and 20 mm is the rolling direction. To cut the samples the guillotine used.

2.6.2 Embedding

Before embedding, due to the thickness of the material (0.35-0.5 mm), it is necessary to glue a piece of some material over the sample to avoid bending (see Fig.5). The sample is glued using a thermosetting sticker that must be heated in an oven during 30 min at 180 º C.

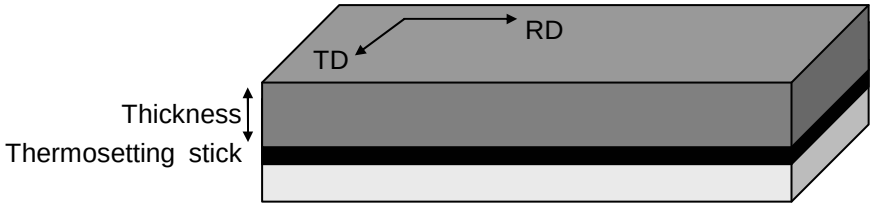

Figure 5 *Texture embedding*

To embed the sample it is used a pre-setup program named Specifast, and a resin with the same name. This program is used because the sample is better glued to the resin than with the durofast.

2.6.3 Grinding and polishing

Following the same procedure than for metallography, the samples are mirror like polished to the 50% of the sheet thickness.

2.7 Texture measurements

2.7.1 Overview of texture analysis

Crystallographic texture is one of the main parameters that characterize the magnetic behavior of electrical steels. The magnetization of the bcc lattice of iron occurs more easily in the <100> than in the <110> or <111> directions, as depicted in the Fig. 6 [7, 8]. Hence, it is interesting to achieve a texture that favours the easier directions.

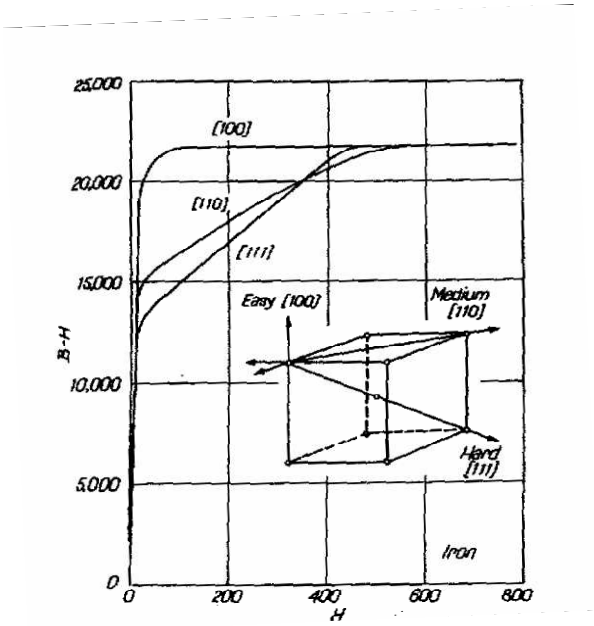

Figure 6 *Magnezitation curves for all single crystal of bcc iron as a function of the crystallographic direction*

2.7.1.1 Representation of Texture

Textures in rolled sheet metals are frequently represented as being of the type {hkl}<uvw>, which means that the {hkl} planes of these grains lie parallel to the plane of the sheet, whereas their directions lie parallel to the rolling direction. It is usual to represent texture in the form of pole figures, which can be determined by using appropriate X-ray diffraction techniques. The information contained in pole figures is incomplete and at best semiquantitative. One way of removing this difficulty is to use the crystallite orientation distribution function (ODF), which essentially describes the frequency of occurrence of particular orientations in a three dimensional (Euler) orientation space.

Considering two reference systems Kc and Ks, as is shown in Fig.7, it is possible to define a function *g* that transforms the reference system of the sample in the crystal system as follows [15, 16]

$$K_c = gK_s \qquad (10)$$

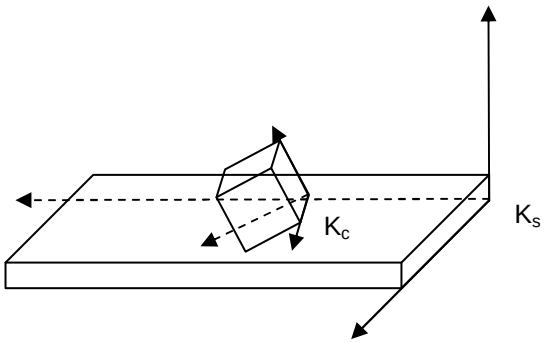

Figure 7 *Reference systems of sample and crystal*

Ks: Sample reference system

Kc: Crystal reference system

The function *g* can be written following the Bunge notation [17], using Euler angles as:

$$g = g(\varphi_1, \phi, \varphi_2) \qquad (11)$$

The Orientation Distribution Function, f(g), is defined as the volume fraction of crystallites with a crystallographic orientation in the infinitesimal interval *g+dg,*

$$f(g)dg = \frac{dV}{V} \qquad (12)$$

In the case of a policrystal f(g) must follow that

$$\oint f(g)dg = 1. \quad (13)$$

While in the case of a monocrystal

$$f(g) = \delta_{Dirac} \quad (14)$$

The orientation distribution function f(g) can be approximately calculated using the 3D Fourier series

$$f(g) = \sum_{l=0}^{L} \sum_{\mu=1}^{M(l)} \sum_{\upsilon=1}^{N(l)} C_l^{\mu\nu} T_l^{\mu\nu} \qquad (15)$$

Where *M(l)* and *N(l)* are the number of independent functions of symmetry of the crystal and the sample, respectively. The coefficients *C* and *T* can be calculated using the four pole figures. Therefore, by means of the pole figure is possible to calculate the orientation distribution function. The Euler space is built varying the angles $\varphi_1, \phi, \varphi_2$ between 0 and 90ºC. On this way, it is possible to generate a dominium as the given in Fig. 8 .

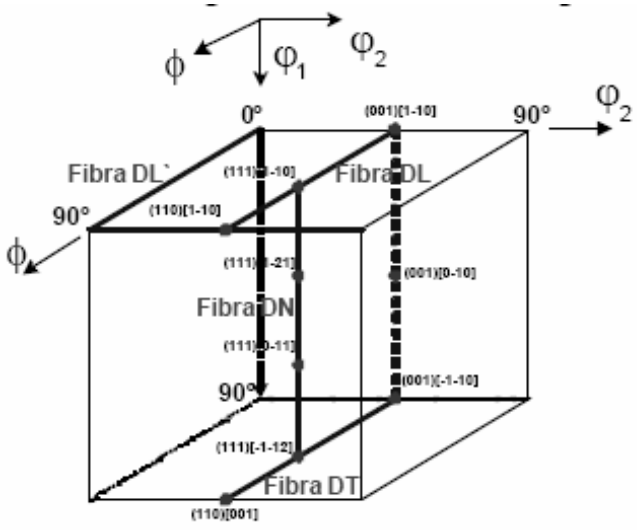

Figure 8 A three-dimensional view of Euler space (Bunge notation)

It is possible to assign a point in this space, to each texture component, using the equations bellow:

$$\varphi_1 = arcsen\left[\frac{w}{\sqrt{u^2+v^2+w^2}}\sqrt{\frac{h^2+k^2+l^2}{h^2+k^2}}\right]$$
$$\phi = ar\cos\left[\frac{1}{h^2+k^2+l^2}\right] \qquad (16)$$
$$\varphi_2 = ar\cos\left[\frac{k}{\sqrt{h^2+k^2}}\right]$$

For texture representation of electrical steels normally it is taken the section φ_2=45º, since the more interesting textures are present on this section, see Fig.9

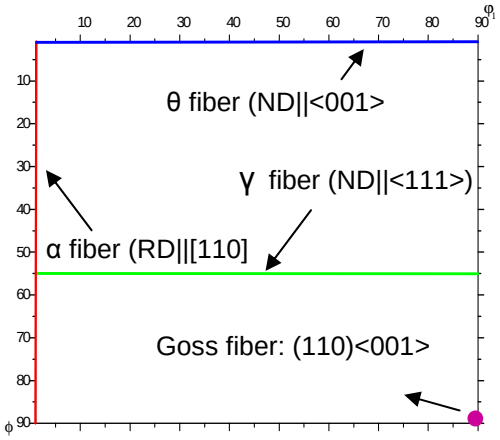

Figure 9 *Section at φ_2=45º*

2.8 Texture measurements

The texture measurements have been performed by means of a Siemens D500 Difractometer. With the software associated to the X-Ray diffractometer it is possible to compute the orientation distribution function, and the volume fraction for each texture. In all the cases the section φ_2=45º has been taken, since it represents the most important textures (γ, α, θ fibers and Goss direction).

2.9 Gleeble tests

In order to simulate the continuous annealing step, Gleeble experiments were performed on a Gleeble 1500 D thermal cycle (Fig. 10).

Figure 10 *Gleeble 1500 D thermal cycle machine*

Fig. 11 shows a schematic illustration of the sample dimensions. To achieve this dimension the steel sheet is first cut with the guillotine and after bended with ERMS 25 100 Haco device. Then a Type S thermocouple is welded at the centre of the samples in order to control and acquire the thermal data. Finally, the sample is clamped in the device, and an electrical current traverses the sample heating it until the desired temperature. All the experiments were performed in a Helium atmosphere to avoid oxidation and/or nitridation.

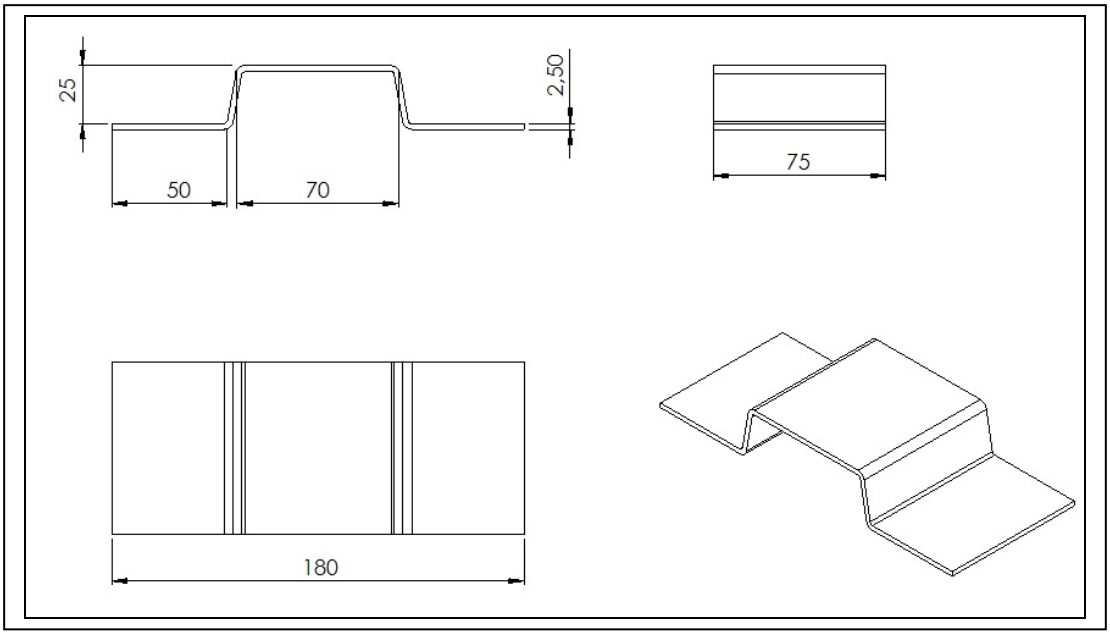

Figure 11 *Sample dimension schematic illustration*

2.10 Magnetic measurements

The magnetic measurements were done by means of a single sheet tester (SST). It is made up of two coils, the primary coil has 170 primary windings and generates the magnetic field, the second one has 280 windings and it is used to measure the induction. The area between the coils is 50x50 mm, therefore, the samples must be cut on these dimensions. In order to cut the samples, they were punched in the Haco Multi 70 Hydraulic Steelsworker.

The magnetic losses at induction levels of 1.0 T and 1.5 T (P10 and P15) are measured, as well as the induction levels in a magnetic field of 2500 A/m and 5000 A/m (B25 and B50) at a frequency of 50Hz. The samples are measured in longitudinal and transversal direction. The reported values are an average of these measurements.

2.10.1 Loss separation

Previously was shown that the total losses can be separated in hysteresis losses (P_{Hys}), Foucault losses (P_F), and Excess losses (P_e).

Hysteresis losses are calculated measuring the hysteresis loop area at 0.1 Hz. Foucault losses (W/Kg) are calculated theoretically using the classical formula:

$$P_F = \frac{\pi^2}{6}\frac{1}{\rho}t^2B^2f^2\frac{1}{d} \qquad (17)$$

Where B is the induction (1,5 T), *f* the frequency (50Hz), *t* the thickness, ρ is the resistivity, and *d* is the density. The values of the density and resistivity are computed using the relations that take into account the alloying in the steel. These relations have been determined at OCAS.

And Excess losses can be computed as:

$$P_e = P_{tot} - P_{hys} - P_F \quad (18)$$

3 Materials

3.1 Influence of Mn, Ni and Cr on low loss electrical steel

To study the influence of Mn, Ni and Cr on a low loss grade, the content of these elements was increased. Three different compositions were taken to analyze the influence of each element: one with low element content, the second one with intermediate content, and the last one with high content.

	Low addition	Intermediate addition	High Addition
%wt. Mn	0.12	0.45	0.94
%wt. Ni	0.019	0.067	0.25
%wt. Cr	0.0024	0.059	0.19

Table 1 *Addition content of the new alloying elements*

3.1.1 Effect of soaking temperature on the magnetic properties and grain size of electrical steels with different chemistries

In this investigation, four Non-Oriented full-hard (non-annealed) Electrical Steel grades were used. They are: A (2,8%Si+Al), B (3.3%Si+Al), C (3.8%Si+Al), and D (4.2%Si+Al) with a final thickness of 0.5 mm the influence of soaking temperature (temperature of continuous annealing) and chemistry on the magnetic properties and grain size was studied. Fig.12 shows the theoretical cycles performed with the Gleeble device to simulate the continuous annealing. The soaking temperature has been varied from 960ºC until 1100ºC, maintaining constant the rest of the parameters: Heating rate=25ºC/s, Cooling rate=15ºC/s and soaking time=60s. The experimental cycles are shown in the appendix.

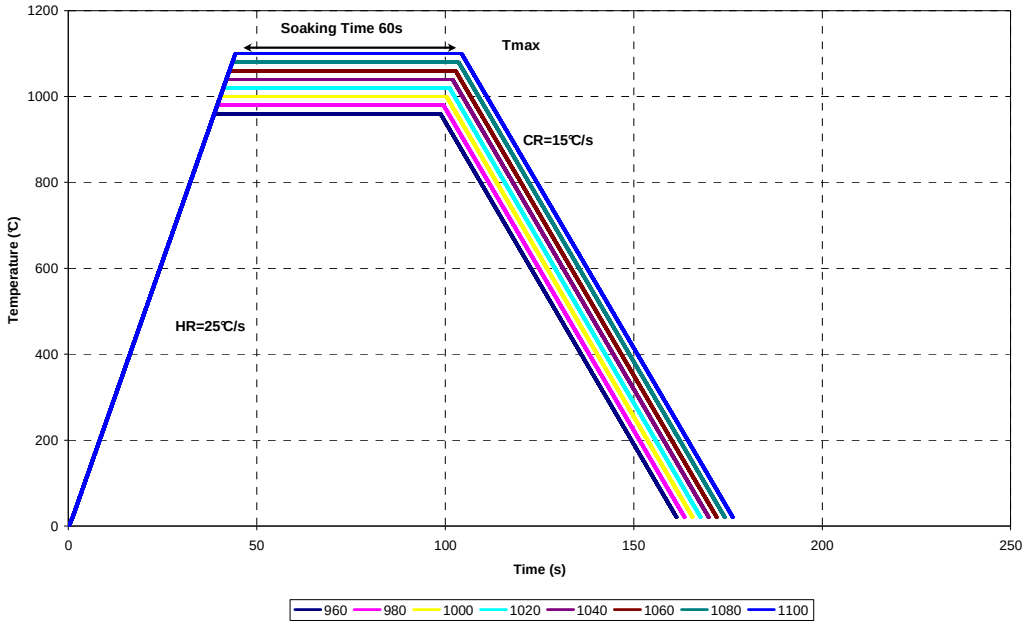

Figure 12 *Target Gleeble test cycles*

4 Results

4.1 Influence of Mn, Ni and Cr on low loss electrical steel

4.1.1 Introduction

It has been widely reported that the addition of some elements like Si or Al have a positive influence on the magnetic properties of steels. Thus, the control of impurities, and the addition of new elements is one of the most important technologies to improve magnetic properties of electrical steels. Previous studies have shown some trends about the influence of Mn, Ni and Cr on the magnetic losses of electrical steels: The magnetic losses decreases linearly with increasing Cr content due to the decrease in eddy current loss through the increase in resistivity [12]. On the other hand, Ni addition appears to increase the final grain size of the material, and thus decrease the losses. Ni element also plays a role in reducing γ fiber during annealing [18]. The influence of Mn is not yet clear, since different studies have arrived to different conclusions. A study performed with 3% Si shows that the grain size increases with the Mn content [21]. While a study performed with 0.5% Si [19] shows that the dependency on Mn content is influence by the S level. In steels containing 0.004 to 0.017%S, an increase in Mn content promotes the grain growth through decreasing the amount of fine manganese sulphide particles. Nevertheless, in ultra-low S steels containing less than 0.001%S, however, the grain growth is inhibited with Mn addition by the precipitation of manganese silicon nitride ($MnSiN_2$). On the other hand, the changes in recrystallization texture being accompanied by grain growth depend only on the Mn content. A higher Mn content results in an increase in {222} component. Increasing Mn content also modifies the mechanical properties, for addition of 0.10% to 0.17% manganese improve the ductility while for addition larger than 0.20% the cold-rolling is difficult and cracks often develop. This fact might be due to the solution hardening effect caused by excess manganese. [20]

4.1.2 Laboratory casting

By means of vacuum casting the materials were mixed to obtain the desired compositions. In a vacuum chamber electrolytic iron (pure iron a small concentration of oxygen) and a small quantity of aluminium is melted. The aluminium reacts with the oxygen producing an aluminium oxide that is evaporated and removed from the vacuum chamber. Afterwards, to achieve the desired concentration FeSi (75% Si) aluminium metallic (pure aluminium), pure Mn, pure Ni and FeCr(70% Cr) are added. Table. 2 shows the measured composition of the low loss electrical steel and the notation used to designate the different alloys

Sample	Notation	C wt.%	Si+Al wt.%	Mn wt.%	Ni wt.%	Cr. Wt.%
Low Mn	B109	0.0034	4.26	0.12		
Intermediate Mn	B110	0.0035	4.37	0.45		
High Mn	B111	0.0044	4.45	0.94		
Low Ni	B112	0.0036	4.31		0.019	
Intermediate Ni	B113	0.0042	4.32		0,.067	
High Ni	B114	0.0043	4.18		0.25	
Low Cr	B115	0.0036	4.29			0.0024
Intermediate Cr	B116	0.0042	4.29			0.059
High Cr	B117	0.0043	4.19			0.19

Table 2 *Addition content of the new alloying elements*

4.1.3 Laboratory processing

For each composition there were two slabs (Group A and B), that follow the same processing steps, in Fig. 15 the process diagram is shown. After the vacuum casting the slabs were hot processed, they were reheated in an oven (see Fig.14) at 1100-1200ºC and hot rolled (see Fig.13) with a finishing temperature in the 800-900℃ range. Afterwards, the y were hot band annealed at 700-800ºC in the laboratories of St. Chely (France). Later, the material was sent back to OCAS-Zwijnaarde where the cold rolling until the desired thickness was carried out. Finally in St. Chely they were continuous annealed at 1000ºC.

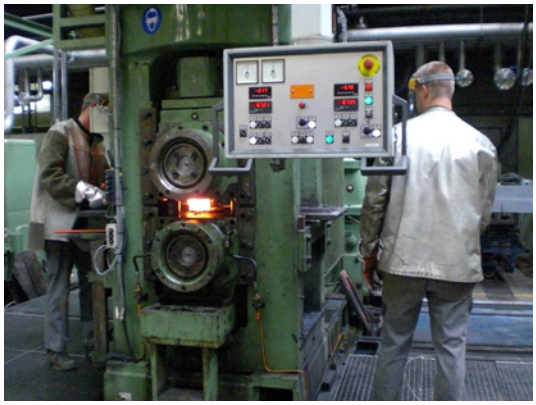

Figure 13 *Hot-rolling and Cold-rolling device*

Figure 14 *Oven to reheat the slabs*

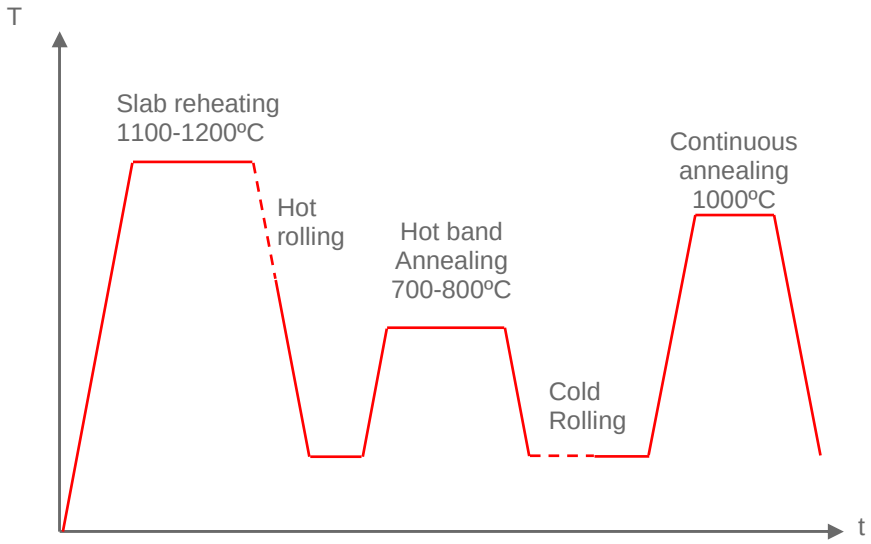

Figure 15 *Laboratory processing steps*

4.1.4 Magnetic properties

The losses P15 and the induction level B50 were measured at 50 Hz, the results are shown in Tables 8 and 9 in the Appendix. The values of P15 and B50 as a function of the different additions are represented in Figs. 16, 17, 18 and 19.

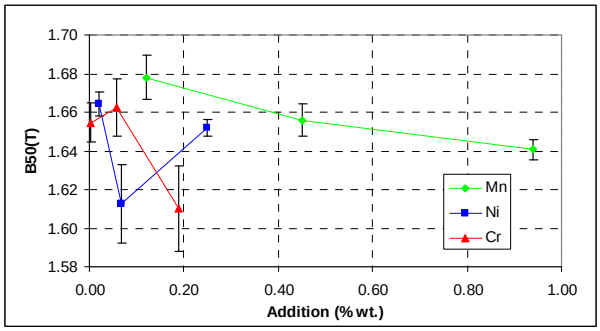

Figure 16 *B50 vs Addition Group A*

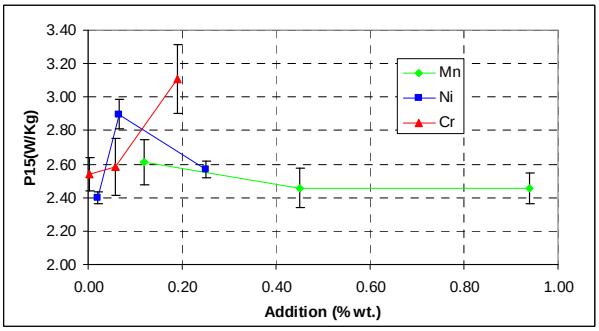

Figure 18 *P15 vs. Addition Group A*

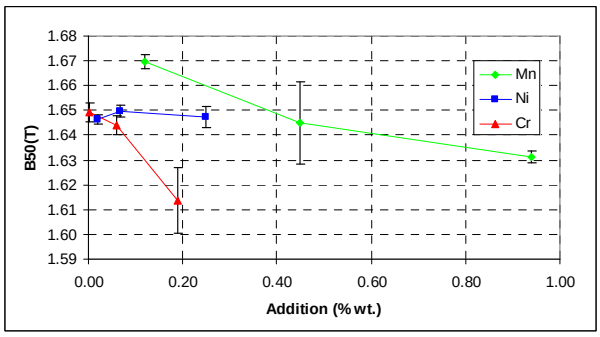

Figure 17 *B50 vs. Addition Group B*

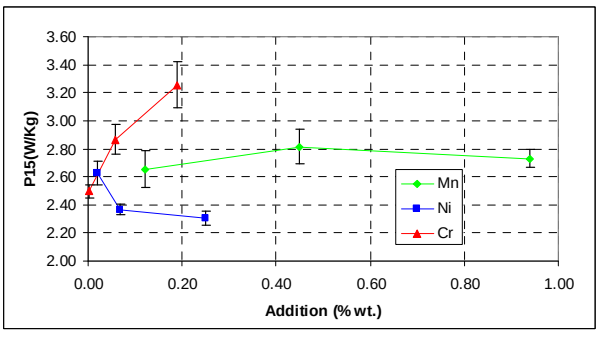

Figure 19 *P15 vs. Addition Group B*

B50 decreases when alloying elements are added to the steel. It is due to a reduction in iron content, and thus in the number of iron atoms and their magnetic moments. Figs. 18 and 19 show that Cr addition increases the magnetic losses. It can be due to two reasons: The formation of Cr precipitates or external oxidation of the sample, since B117 sample has a thicker oxide scale than B115. On the other hand, the addition of Ni has a different influence in Group A and B. While in group A P15/50 does not appear to have a regular behaviour. In the case of group B, Ni appears to be positive for the magnetic losses, since P15/50 decreases approximately 0.4 W/kg. Finally for Mn addition groups A and B have different behaviours: P15/50 in group A decreases, while in group B increases. Nevertheless, in both groups the influence of Mn is smaller than that of Ni or Cr.

In section 4.1.2 the composition of the analyzed samples was shown. It is noticed that not only Mn, Ni and Cr contents vary but also the rest of alloying elements, like Si + Al. This variation achieves differences on Si+Al content of up to 0.2-0.3 (B109-B111). This variation on the composition can also affect the final properties of the material. On the other hand, while Group A and B have the same composition, the magnetic losses show a different behaviour. The difference can be due to the fact that the processing followed by both groups is not identical, since they are two different slabs. Therefore the variation on the process parameters and the composition limit the reproducibility of the experiment.

4.1.4.1 Hysteresis losses

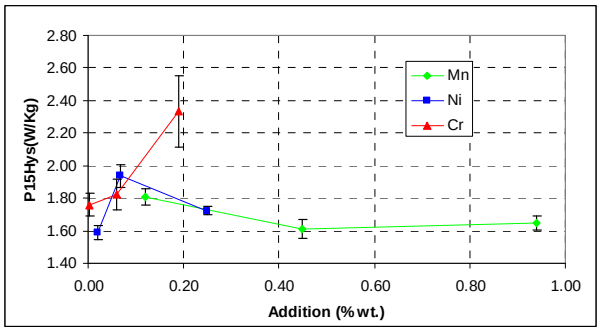

Figure 20 *$P15_{Hys}$ vs. Addition Group A*

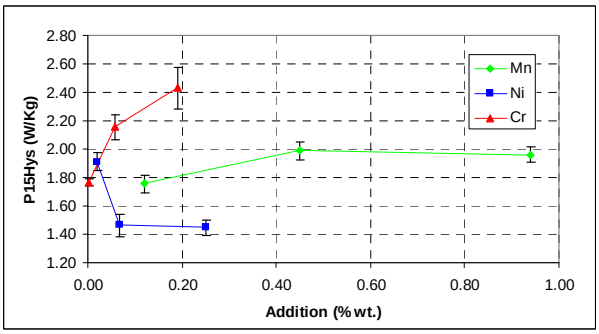

Figure 21 *$P15_{Hys}$ vs. Addition Group B*

The behaviour of the hysteresis losses is similar to that of the total losses. It means that the total magnetic losses behaviour is mainly due to hysteresis losses.

4.1.4.2 Foucault losses

Fig. 22 shows the calculated values of the resistivity using the OCAS formulas. The resistivity depends only on the composition of the material; hence, the values of the resistivity are equal in group A and B. It can be seen that in the considered content range, Mn is the element with the higher

influence in the resistivity. The studied variations in Ni and Cr have a negligible effect on the resistivity.

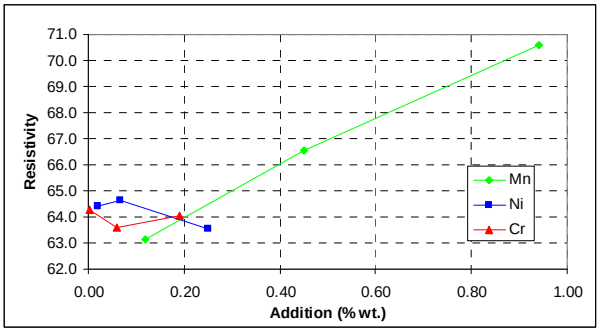

Figure 22 *Resistivity vs. Addition*

Foucault losses are calculated theoretically, using the measured thickness values. Therefore, the difference between group A and B is given by the difference in thickness.

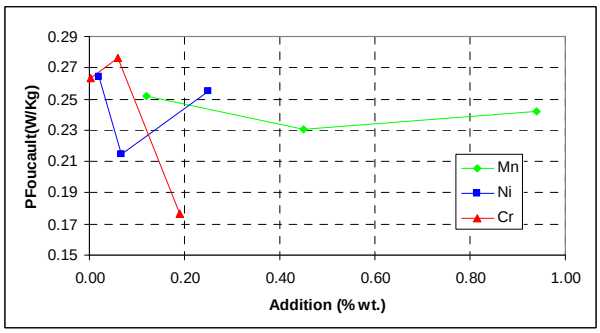

Figure 23 *P_F vs. Addition Group A*

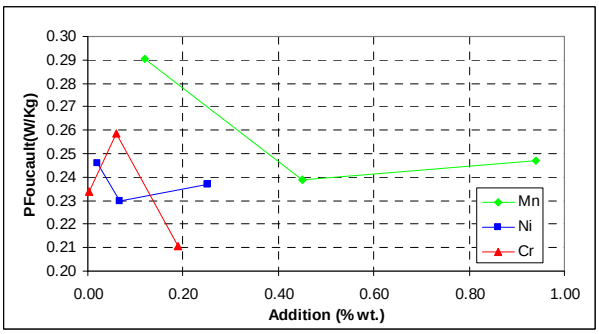

Figure 24 *P_F vs. Addition Group B*

Despite of the increase on resistivity, the Foucault losses do not decrease as it was expected. This is due to differences in the thickness between the samples.

4.1.4.3 Excess losses

Figs. 25 and 26 show the calculated excess losses

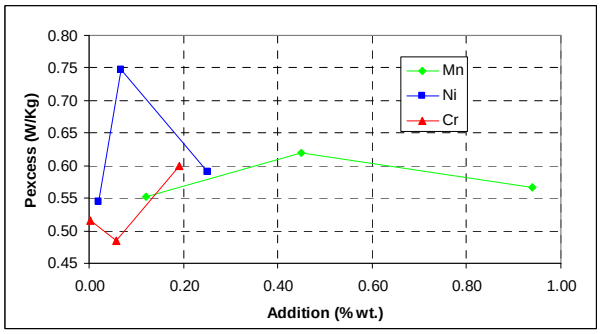

Figure 25 *P_e vs. Addition Group A*

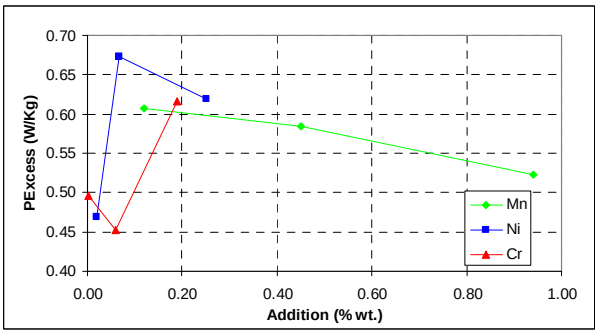

Figure 26 *P_e vs. Addition Group B*

Excess loss shows often more scattered values.

4.1.5 Microstructural analysis

The microstructures after hot rolling (HR), hot band annealing(HB) and continuous annealing(CA) have been analyzed. Figs. 27, 28, and 29 show some representative images of the microstructures:

	Low Mn	Intermediate Mn	High Mn
HR	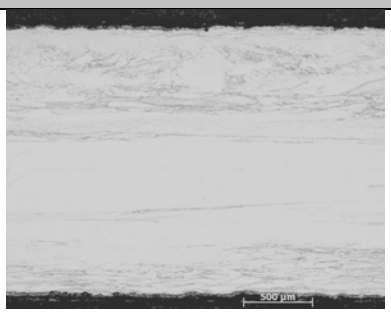		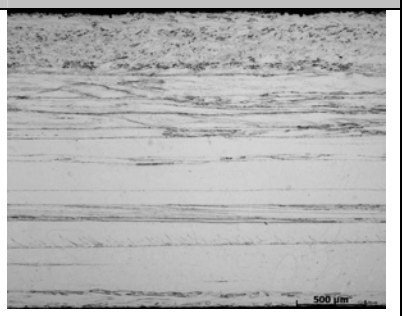
HB	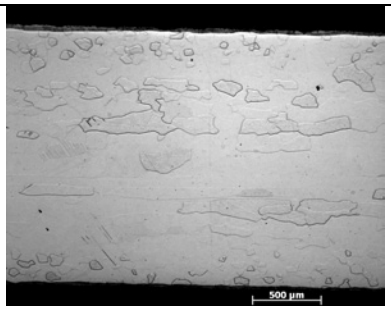	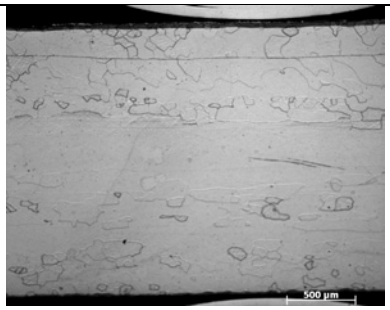	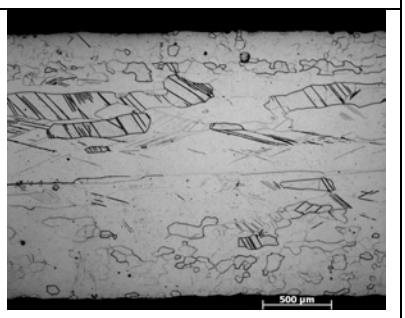
CA	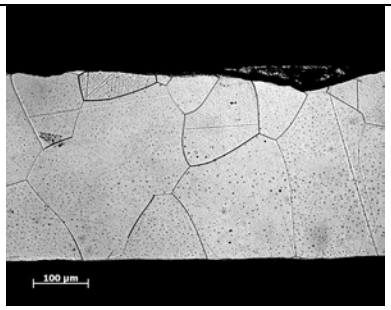	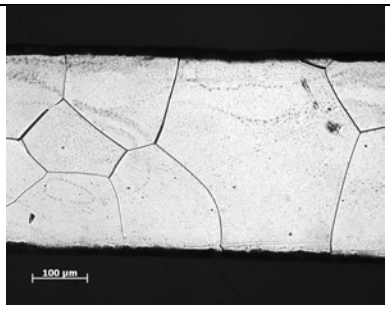	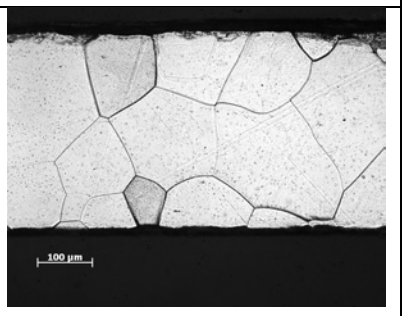

Figure 27 *Microstructure of steels with different Mn-contents*

	Low Ni	Intermediate Ni	High Ni
HR		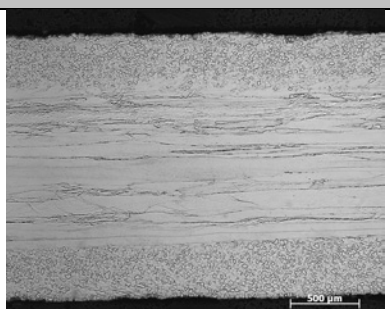	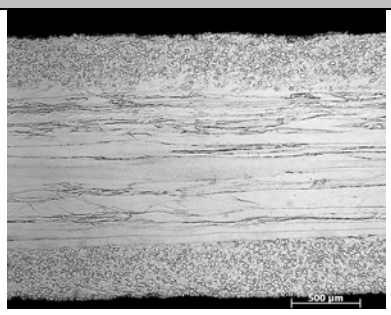

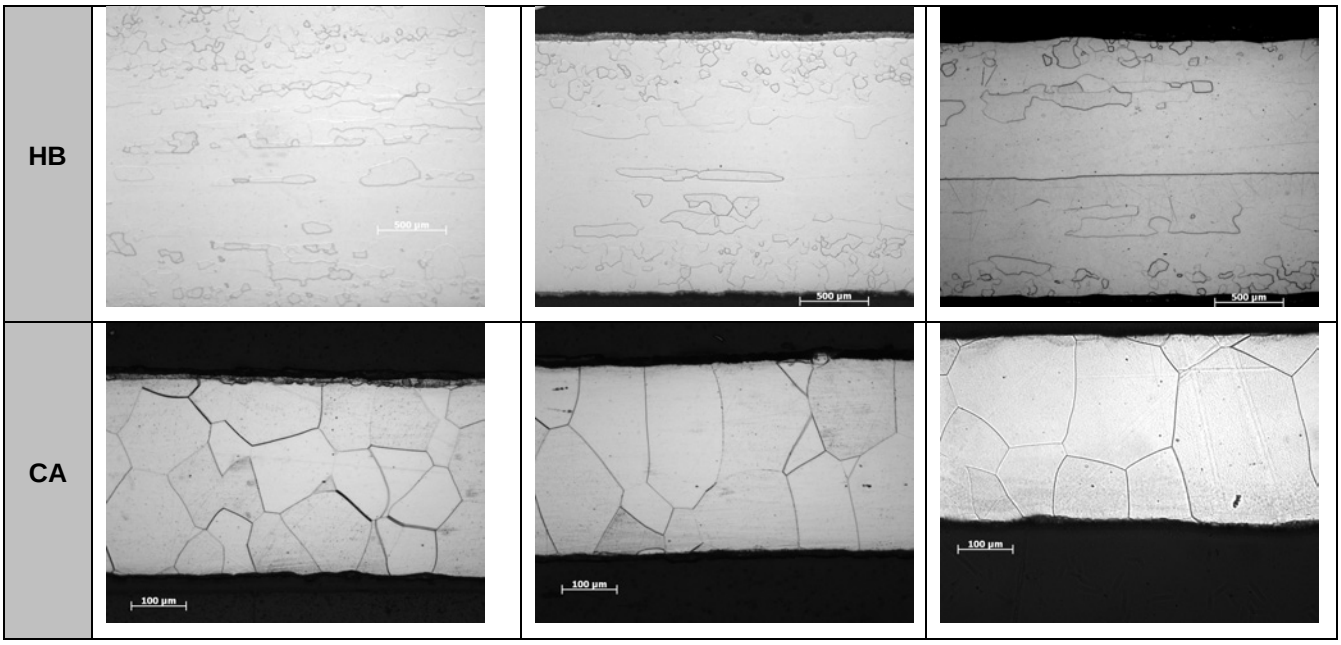

Figure 28 *Microstructure of steels with different Ni-contents*

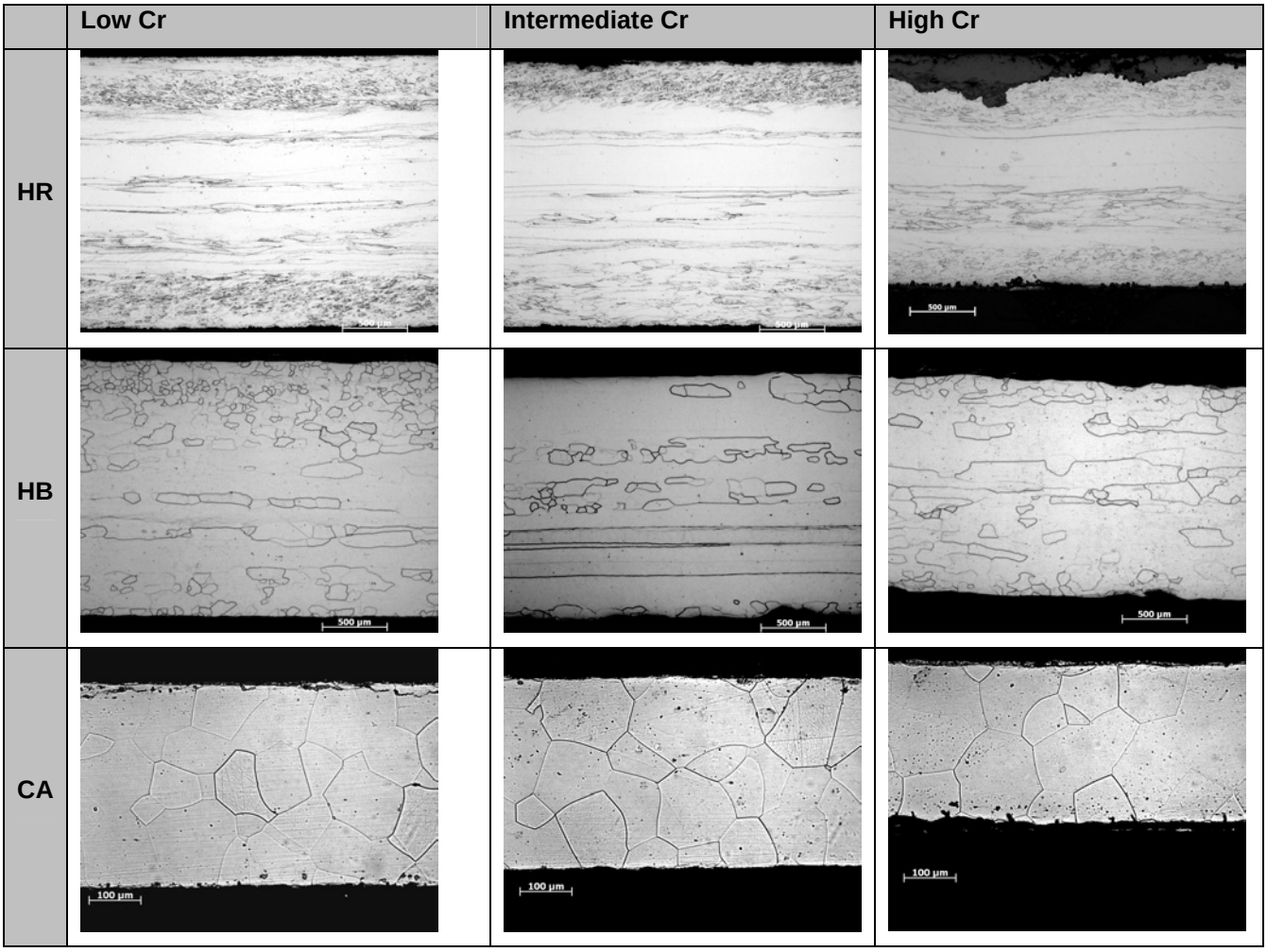

Figure 29 *Microstructure of steels with different Cr-contents*

After hot rolling B113 and B114 samples (Ni addition) are partially recrystallized, this fact can be due to two facts: that Ni accelerates the recrystallization or that during the hot-rolling process there was some variation in the processing parameters.

When Mn content is increased cracks appear in the middle of the sample (see Figs. 30 and 31).This fact matches with the previous studies that indicate that the addition of Mn deteriorate the mechanical properties, promoting the appearance of cracks.

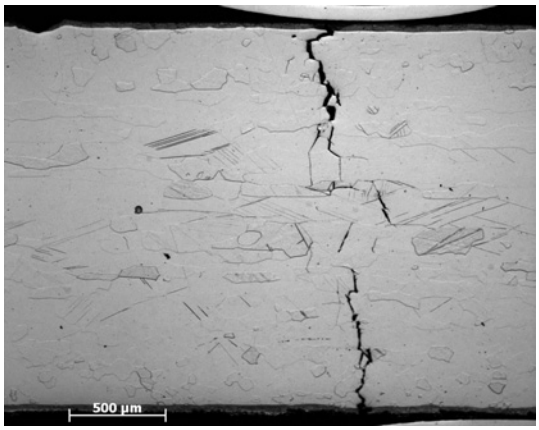

Figure 30 *Cracks on High Mn sample*

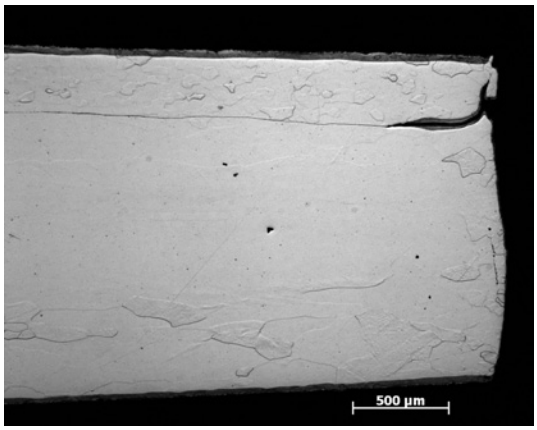

Figure 31 *Cracks in Intermediate Mn sample*

High Cr sample presents a larger oxide scale that is reflected in a final thickness of 0.30 mm instead of the expected 0.35 mm

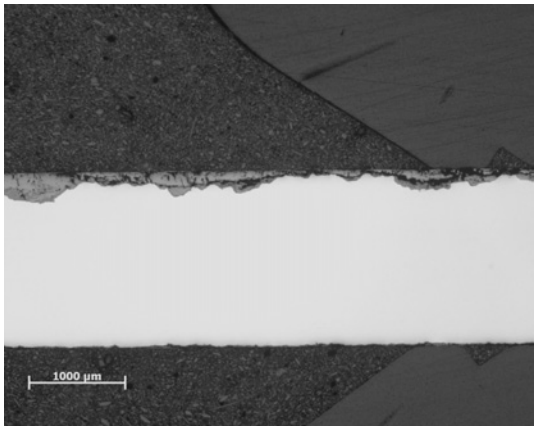

Figure 32 *Oxide scale of High Cr sample*

Using the intercept procedure the *grain size* after continuous annealing was measured; the results are shown in Table 8 and 9 (Appendix). In Figs. 33 and 34 the mean diameter is represented as a function of the alloying additions for group A and B, respectively.

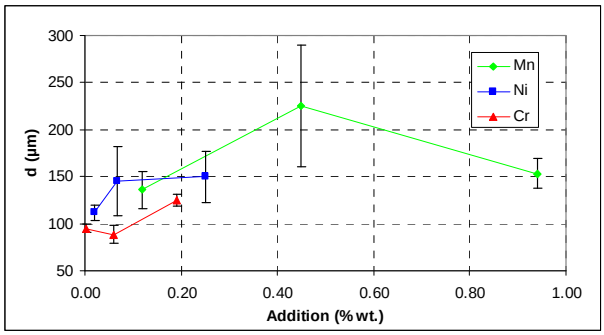

Figure 33 *Grain size vs. addition Group A*

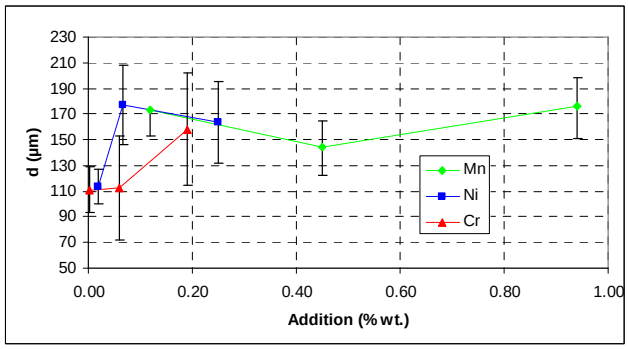

Figure 34 *Grains size vs. Addition Group B*

Observing the previous graphs we can conclude that Cr addition has a positive effect, since the grain size increases. On the other hand, for Ni addition the grain size seems to increase for the intermediate Ni addition, but when the Ni content is increased it appears to remain constant or even decrease. Finally for Mn addition, it is difficult to predict the behaviour for the intermediate addition, since in group A and B the behaviour is totally different, and the error associated to the measure is huge. But comparing the low content sample with the high content sample, we can assume that Mn content has a low contribution to increase grain size.

4.1.6 Texture

Table 3 gives an overview of the ODF (Orientation Distribution Function) section at φ_2=45° at half plate thickness for samples of group B. Table. While Table 4 shows α, γ, θ and Goss volume fraction as well parameter θ/γ for those samples.

	Low	Intermediate	High
Mn	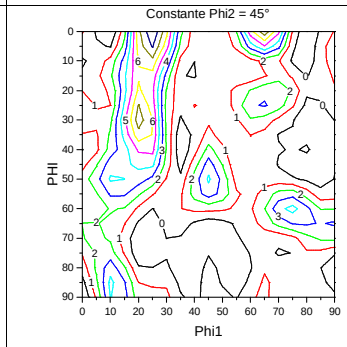	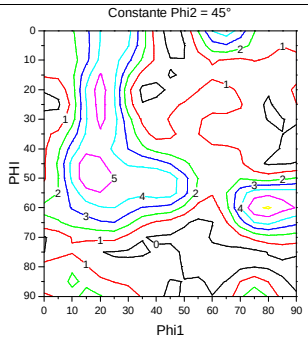	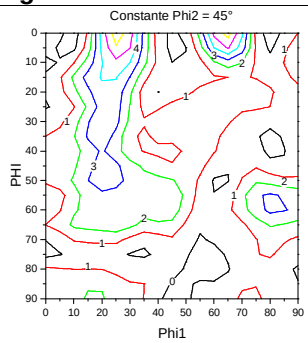
Ni	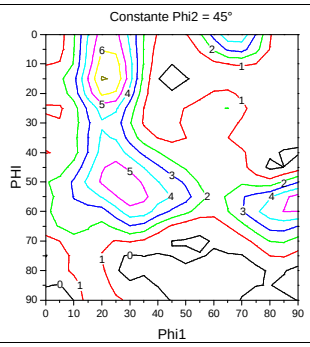	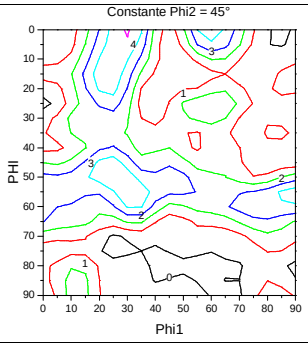	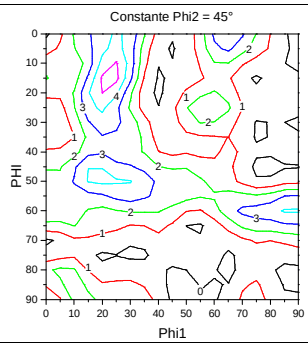
Cr	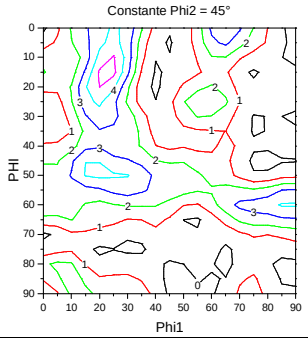	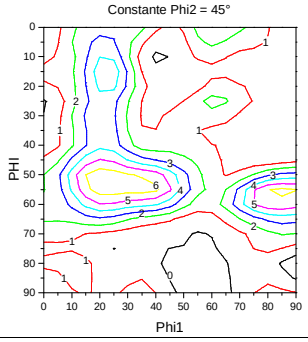	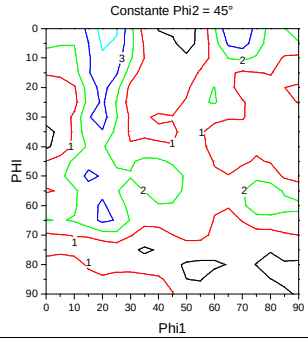

Table 3 *Group B ODF sections at φ2=45º*

Sample	Notation	α fraction	θ fraction	γ fraction	Texture factor θ/γ
Low Mn	B109B	42.60	63.10	52.60	1.20
Intermediate Mn	B110B	47.08	62.40	85.30	0.73
High Mn	B111B	36.69	61.85	58.60	1.06
Low Ni	B112B	40.99	51.99	89.31	0.58
Intermediate Ni	B113B	43.50	61.01	79.14	0.77
High Ni	B114B	46.31	60.26	67.29	0.89
Low Cr	B115B	39.57	64.99	82.59	0.79
Intermediate Cr	B116B	43.09	55.67	79.70	0.70
High Cr	B117B	47.61	61.15	63.70	0.96

Table 4 *α , γ, θ volume fraction as well θ/γ texture factor*

In Fig. 35 the texture factor θ/γ as a function of the addition of Mn Ni and Cr is represented

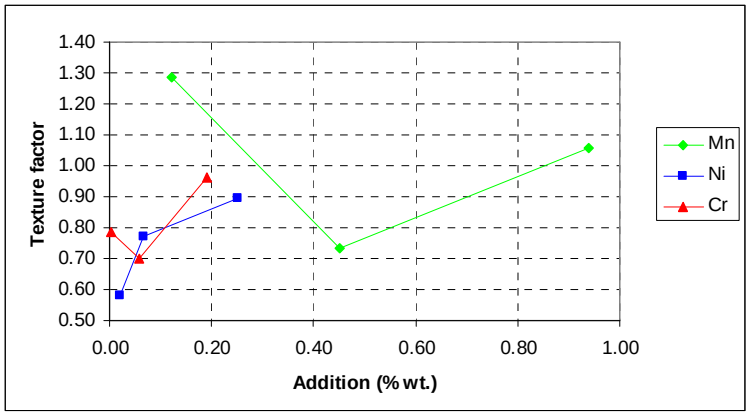

Figure 35 *Texture factor vs. addition of Group B*

B109B and B111B samples (low and high Mn) have a pronounced peak of intensity in the θ component, while it is almost absent in B110 (intermediate Mn). This fact corresponds with a higher texture factor for B109B and B111B than for B110B.

In the case of Ni addition, texture factor increases when Ni content augments. It is due to a decrease on γ fibre intensity (see Table. 15) . Therefore, Ni appears to inhibit the formation of γ-fibre.

For Cr addition the texture factor has not a regular behaviour. B116B ODF section shows as strong γ fibre, while for B117B it has disappeared and emerge a small peak on θ fibre.

4.1.6.1 Study of the texture homogeneity

After cold-rolling the steel plates has a length of approximately 75cm (each plate has different dimensions). Due to the large dimensions of the plate it is interesting to study the homogeneity of the plate. With this objective, it was studied the texture homogeneity of the B109B sample along the plate. Three samples were analysed at 10%, 40%, and 80% of the length. In Figs. 36, 37 and 38 the ODF sections are shown:

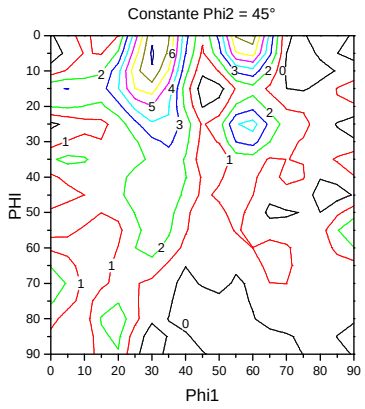

Figure 36 *B109B 10%*

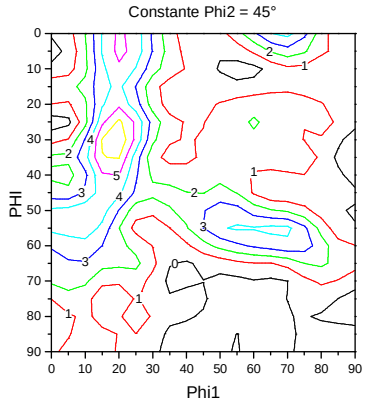

Figure 37 *B109B at 40%*

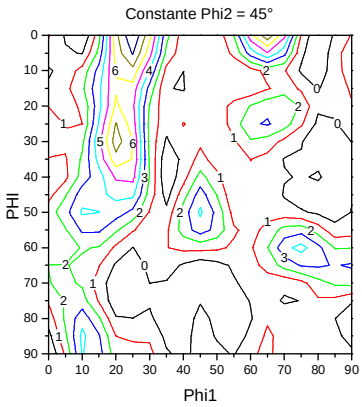

Figure 38 *B109B at 80%*

Sample	α volume fraction	θ Volume fraction	γ volume fraction	Texture factor θ/γ
10%	33.89	81.29	41.48	1.96
40%	52.06	51.56	67.49	0.76
80%	42.57	63.10	52.61	1.20

Table 5 *Textures values of B109B at 10%, 40% and 50% of the length*

In the ODF sections at 10%, 40% and 80%, we can see that the sample is very inhomogeneous. At 10% of the length it has a pronounced θ fibre peak, and very low intensity on γ. At 40% of the length θ fibre appears to be transformed in γ fibre. While for 80% both γ and θ fibres are present.

4.1.7 Results correlations

The correlations between total losses and *grain size* are shown in Figs.39 and 40. Ni and Mn samples do not appear to have a relation between the total losses and the grain size. Therefore, the difference in the magnetic losses are not due to an increase of grain size. In the case of Cr losses increase when grain size grows.

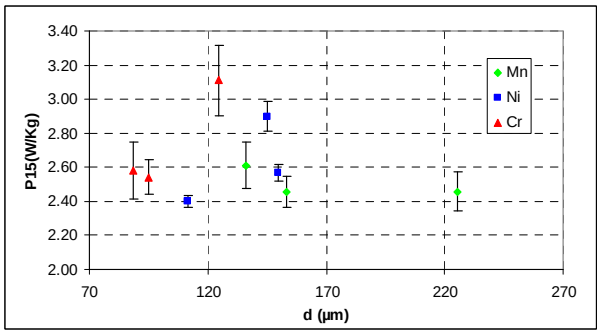

Figure 39 *P15 vs. grain size Group A*

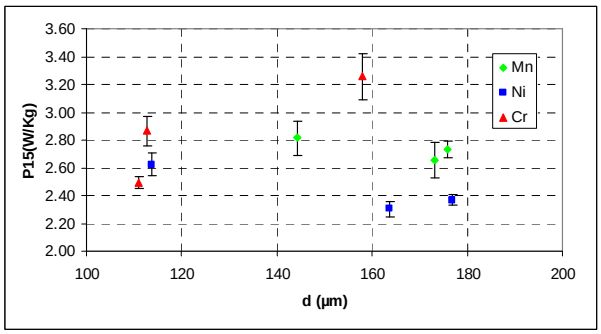

Figure 40 *P15 vs. grain size Group B*

Fig.41 shows the influence of *texture* on the total losses. Total losses generally decrease when texture factor augments. The only exception is the sample with high Cr, but this sample has a thicker oxide scale that can increase the magnetic losses, regardless the texture.

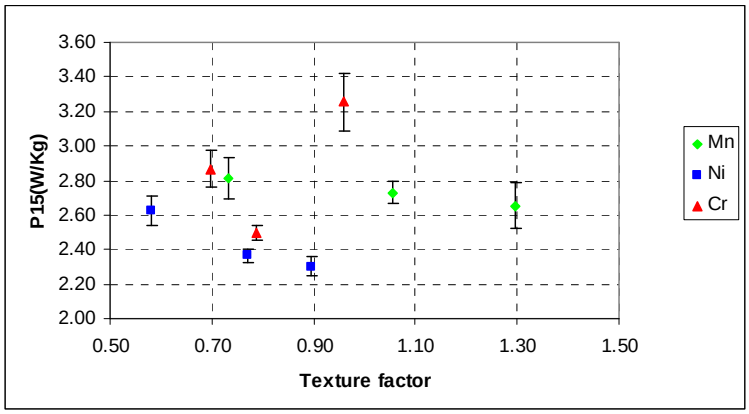

Figure 41 *P15 vs. Texture factor at group B*

4.2 Effect of soaking temperature on the magnetic properties and grain size of electrical steels with different chemistries

4.2.1 Introduction

4.2.1.1 Effect of grain size on the magnetic properties

The effect of grain size on magnetic properties of silicon steel was first studied by W.E. Ruder in 1912, who discovered that the hysteresis loss decreases as the grain size is coarsened [5]. Since then, the influence of grain size has been studied [6]. However, the results of their researches are not universally applicable, since they are essentially subject to the effects of steel purity and oxidized surface layer.

Table 6 summarizes 12 reports referring to grain sizes which should offer minimum core loss in electrical steel sheets. The data given in table 6 indicates that minimum core loss is obtained at a grain diameter of 130 to 220 µm regardless of silicon content.

Report No.	Si (wt%)	Thickness	Core Loss	Optimal Grain Size	Remarks
7 (1972)	0		$W_{10/60}$	169 μm	
			$W_{15/60}$	163 μm	
8 (1973)*	~3	0.5 mm	$W_{10/50}$	Between 240 and 260 μm	Electric-arc furnace
			$W_{15/50}$	ditto	
	~3	0.5 mm	$W_{10/50}$	Between 370 and 390 μm	Open-hearth furnace (substantial
				ditto	amounts of sulfides and oxides)
9 (1977)	3.2	0.5 mm	$W_{10/50}$	Between 175 and 275 μm	
10 (1979)	2	0.5 mm	$W_{10/50}$	Approximately 180 μm	Core loss 1 + C + 2·45 deg (av-
					erage)
11 (1981)	0	0.5 mm	$W_{15/60}$	Between 50 and 190 μm	
12 (1981)	1.85	0.5 mm	$W_{15/50}$	Approximately 90 μm	
	2.8	0.5 mm	$W_{15/50}$	Approximately 110 μm	
	3.2	0.5 mm	$W_{15/50}$	Approximately 140 μm	
13 (1982)	3.2	0.5 mm	$W_{15/50}$	Between 100 and 150 μm	
14 (1984)	3.2	0.5 mm	$W_{10/50}$	Approximately 150 μm	
15 (1984)	~2	0.53 mm	$W_{15/60}$	Between 50 and 200 μm	
16 (1985)	3.2	0.5 mm	$W_{15/50}$	Approximately 110 μm	Ordinary steel
	3.2	0.5 mm	$W_{15/50}$	Approximately 150 μm	Super high purity steel
17 (1987)	0	0.61~	$W_{10/60}$	180 μm	
		0.71 mm	$W_{15/60}$	130 μm	
			W_{15} DC	100 μm	
18 (1987)	3.3–3.5	0.5 mm	$W_{15/50}$	Approximately 100 μm	

*Hot rolled electrical steel sheets.

Table 6 *Grain size offering Minimum Core Loss [6]*

4.2.1.2 Effect of annealing conditions on the magnetic properties

Annealing treatment is needed to relieve the residual stress and develop the grain growth and proper texture and thus the required combination of core loss and permeability is obtained. However, the effect of this treatment is known to be very sensitive to operating conditions, such as temperature and time, type of atmosphere,…etc [9]. Therefore, controlling these conditions to the optimum state is considered very important to fully take advantage of annealing.

4.2.1.3 Oxide scale formation

Core loss is strongly affected by the oxidation occurring during the final heat treatment. The oxide reaction is affected by the composition of the material, the temperature of the heat treatment and the atmosphere in the furnace [14].

The influence of silicon on the oxide scale structure depends on the range of temperature considered [3]. In FeO-Si-O_2 phase diagram the oxides involved in the oxide scale formation can be observed, for iron-silicon alloys. The oxides involved are: SiO_2, Fe_2SiO_4, FeO, Fe_3O_4 and Fe_2O_3.

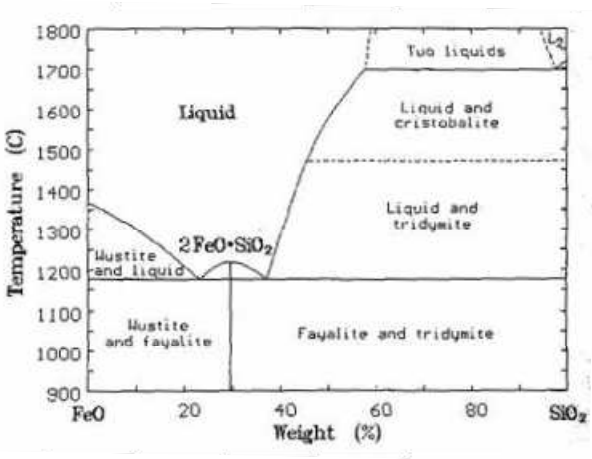

Figure 42 *FeO-SiO_2 binary system*

At low silicon contents, SiO_2 is formed at the alloy surface, distributed very finely. Simultaneously, it reacts with FeO to form fayalite, Fe_2SiO_4, and when the SiO_2 particles become larger, they are engulfed by the scale. Fayalite particles are often aligned parallel to the surface (Fig.43)

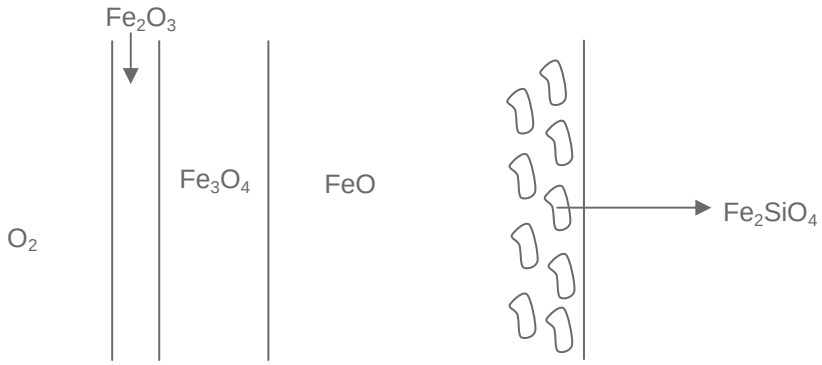

Figure 43 *Schematic representation of the scale formed on Fe-Si alloys*

Another important element that influences the composition of the oxide scale is Aluminum [2]. It was studied the oxide scale formation by decarburation, for sheets annealed in H_2O-N_2 gas mixture and temperature between 800ºC and 1050ºC, and was demonstrated that for high Al alloyed sheets (2%wt. Si and 1%wt. Al), the oxides involved in the oxidation are FeO, Fe_3O_4 , Al_2O_3 , Hercynite ($FeAl_2O_4$), and Fayalite Fe_2SiO_4.

4.2.2 Magnetic properties

Fig. 44 shows the magnetic losses, P15/50, as a function of the soaking temperature (see the measured data in the appendix)

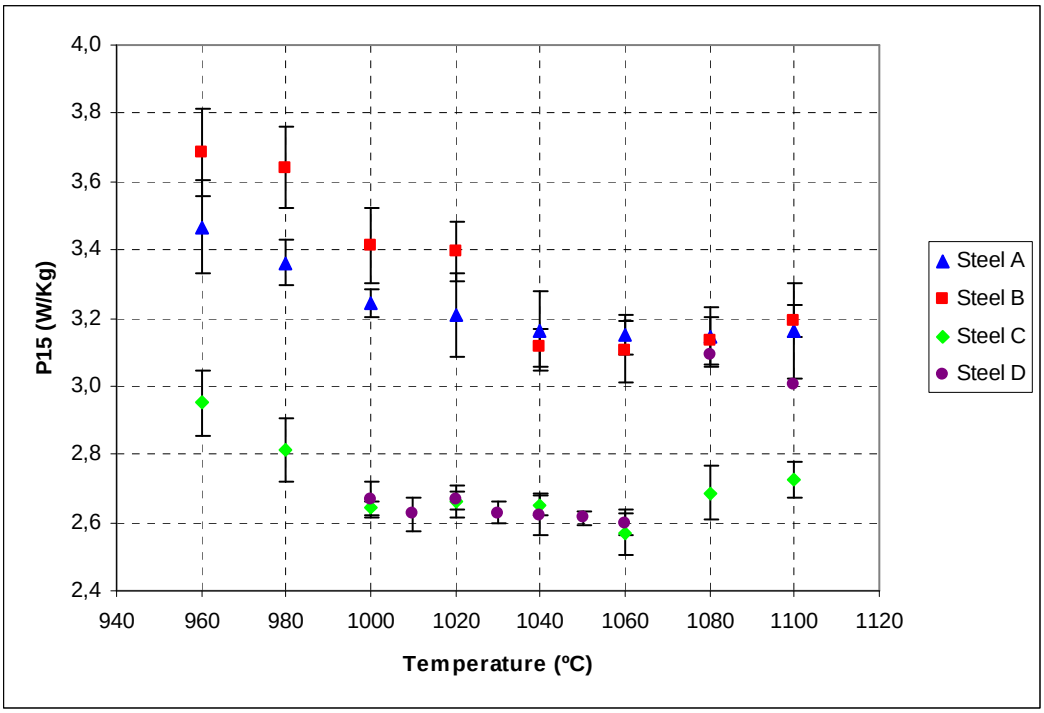

Figure 44 *P15 vs. soaking temperature*

In the range of low soaking temperatures losses decrease when the soaking temperature increases, but it reaches a minimum that varies depending on the composition. In the case of Steel B the minimum is in the range 1040-1060ºC, Steel A is in the range 1040-1080ºC and Steel C in the range 1020-1060ºC. Note that Steel D has a strange behaviour for soaking temperatures of 1080 and 1100ºC; this fact probably is due to some experimental error. Therefore, these points will not be considered in the posterior analysis.

As it was expected Steel C and D have lower magnetic losses than Steel A and B, since they have a higher Si and Al content. However, when Steel A is compared with Steel B an unexpected effect is seen, since for low temperatures Steel A has lower magnetic losses than Steel B, in spite of the lower content of Si+Al.

4.2.3 Grain size

The grain size after the continuous annealing has been measured; the results obtained are shown in Appendix. Fig.45 shows the grain size as a function of the soaking temperature.

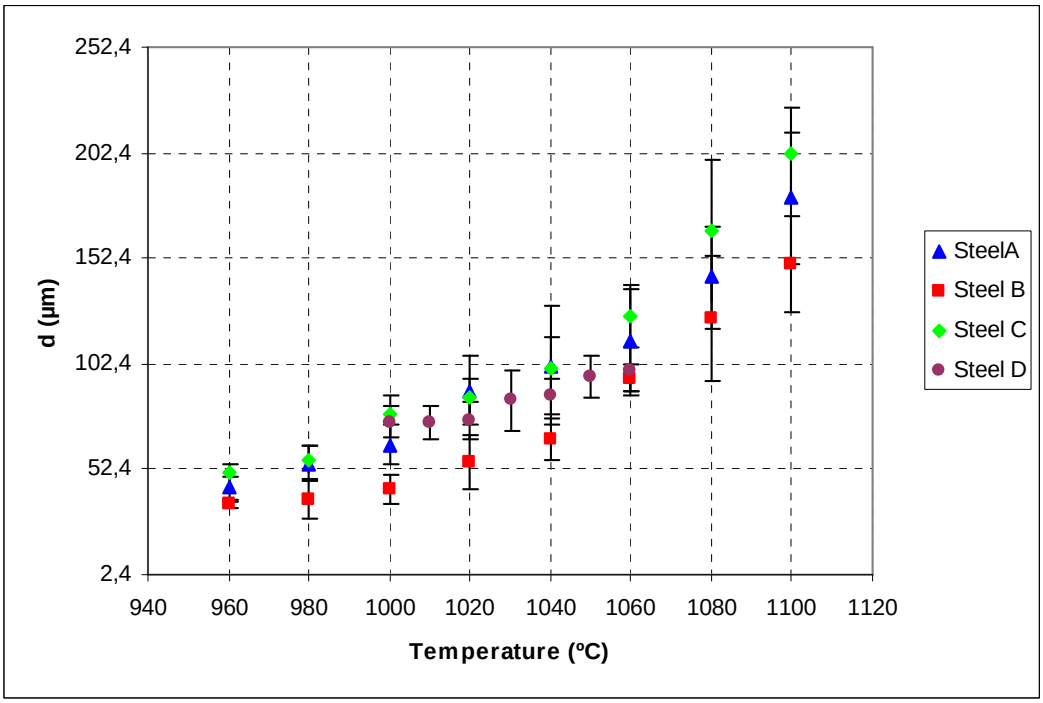

Figure 45 *Grain size vs. soaking temperature*

Grain size always increases when the soaking temperature is increased, but the slope of the curve depends on the composition of the sample. The data obtained can be used to build a model to predict the behaviour of the materials with the soaking temperature.

4.2.3.1 Grain size modelling

The kinetics of grain growth during recrystallization of ferrite is a function of reduction percent in the cold rolling (thickness) and the annealing parameters (soaking time and temperature). Grain size can be modelled following the Arrhenius law:

$$D = \frac{K_{rec}}{\%red} + K_0 t^{0.25} \exp\left(\frac{-E_A}{RT}\right) \qquad (19)$$

Where, t is the soaking time (60s), T the soaking temperature, R is the Boltzmann constant(8.31 J/Mol.K), E_A is the activation energy of grain growth, K_0 is a constant independent of the temperature, and $\frac{K_{rec}}{\%red}$ is the grain size before second recrystallization. % red is the reduction percent in the cold-rolling (0.75) and is given by:

$$\%red = \frac{d - d_0}{d_0} \qquad (20)$$

Excel software was used to calculated the optimum constants to approximate the equation to the experimental data.

	Steel A	Steel B	Steel C	Steel D
K_{rec} (µm)	12.18	14.25	23.40	-
K_0	16.10^7	35.10^9	80.10^8	-
E_A (J/mol)	169627	232908	213206	-
R^2	0.99	0.99	0.99	-

Table 7 *Modelling parameters*

It is not possible to fit the experimental data to the Arrhenius law for Steel D sample with a high regression factor, it is due to the lack of points at high temperatures.

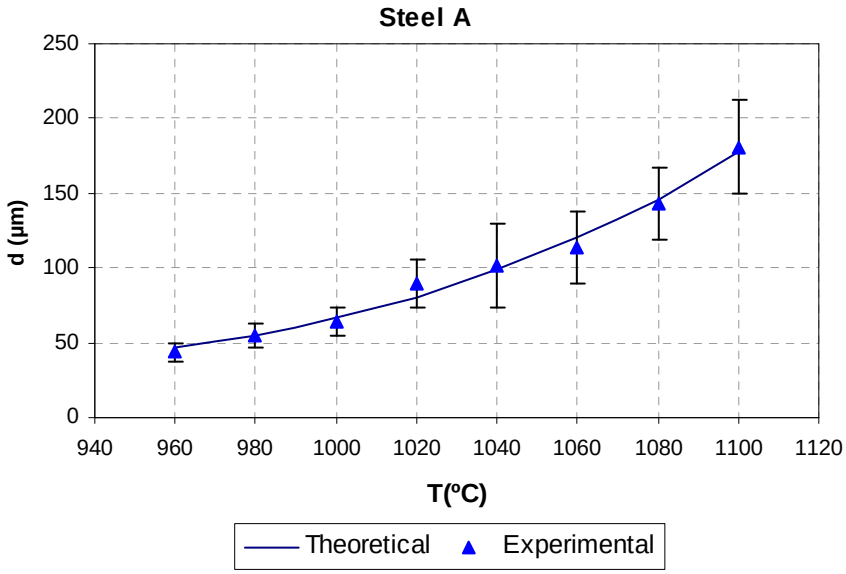

Figure 46 *Model of grain size vs. soaking temperature for Steel A*

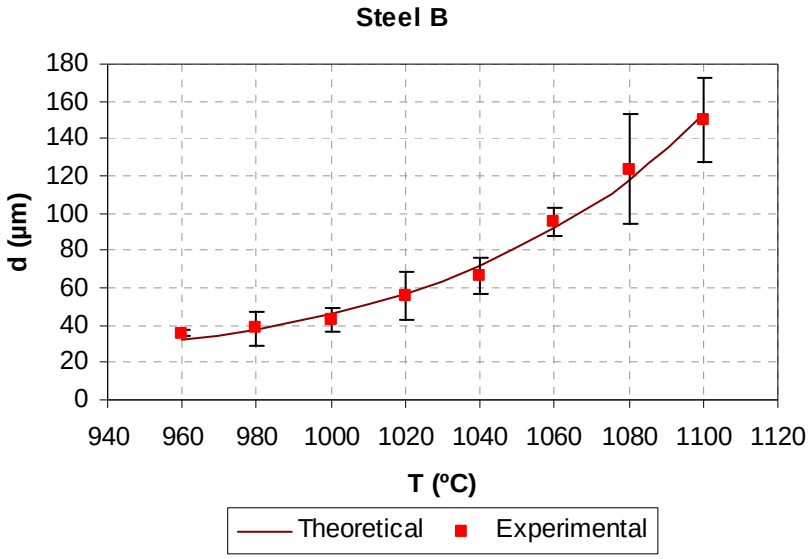

Figure 47 *Model of grain size vs. soaking temperature for Steel B*

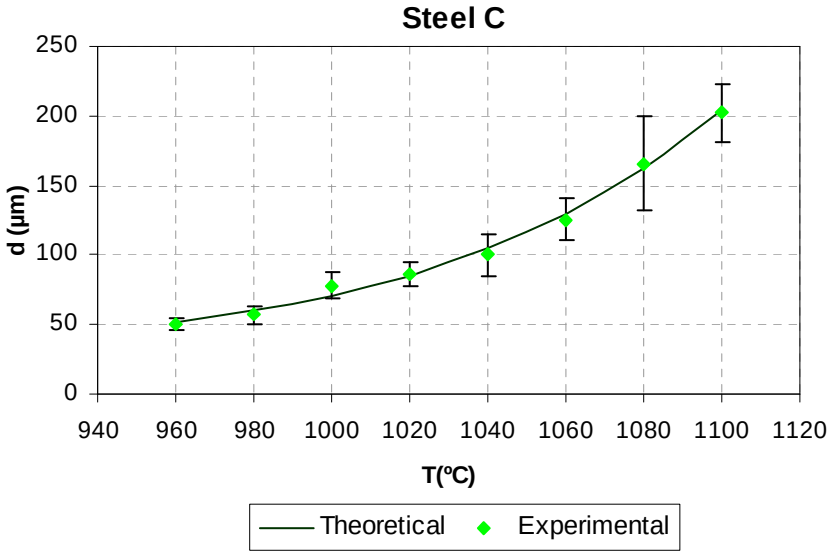

Figure 48 *Model of grain size vs. soaking temperature for Steel C*

Table 7 shows the model constants calculated. It can be seen that Steel C has a higher grain size before cold-rolling than Steel A and Steel B; it is due to the fact that unlike Steel A and Steel B, Steel C was subjected to hot band annealing. From 1060ºC the samples present an acceleration of the grain growth process

4.2.4 Correlation between P15 and grain size

Fig. 49 shows the magnetic losses as a function of grain size.

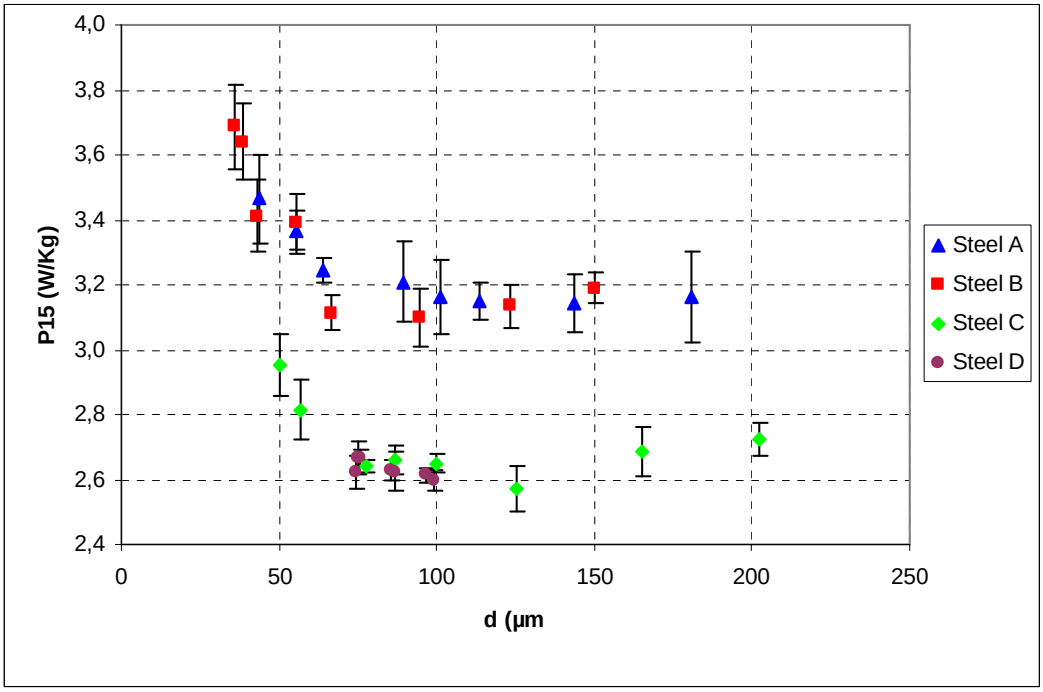

Figure 49 *P15/50 vs. grain size*

A pronounced decrease on the magnetic looses with the grain growth is observed for low values of the grain size. However, when it achieves values around 90-130 µm the decrease stops, obtaining a minimum in the magnetic looses.

4.2.5 Oxidation

The influence of the soaking temperature and the composition on the oxide scale formed during annealing has been analyzed. Four samples have been examined: Steel D material at soaking temperatures of 1000ºC and 1060ºC and Steel B at the same temperatures. The oxide scale of the samples has been observed by electron microscopy. Some representative SEM images of the oxide scales of the four samples are presented below. The analysis of the composition has been performed by means of X-Ray diffraction (EPMA and SEM devices).

Steel D-1000

Shape

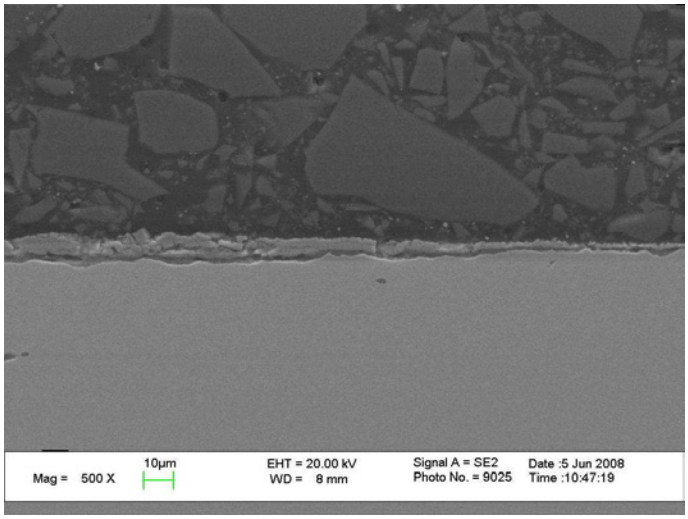

Figure 50 *Steel D-1000 SEM image at 500x*

Composition

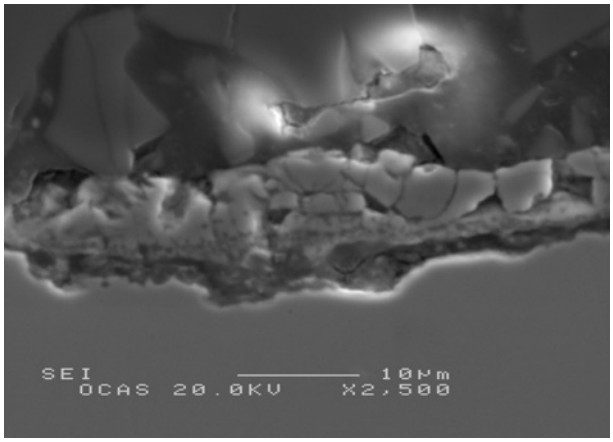

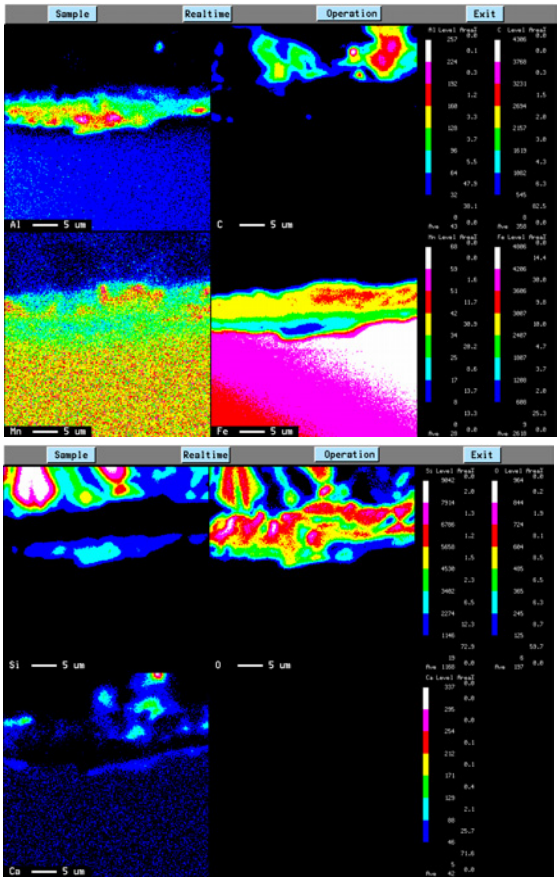

Figure 51 *Steel D-1000 EPMA XRD mapping*

Internal oxidation

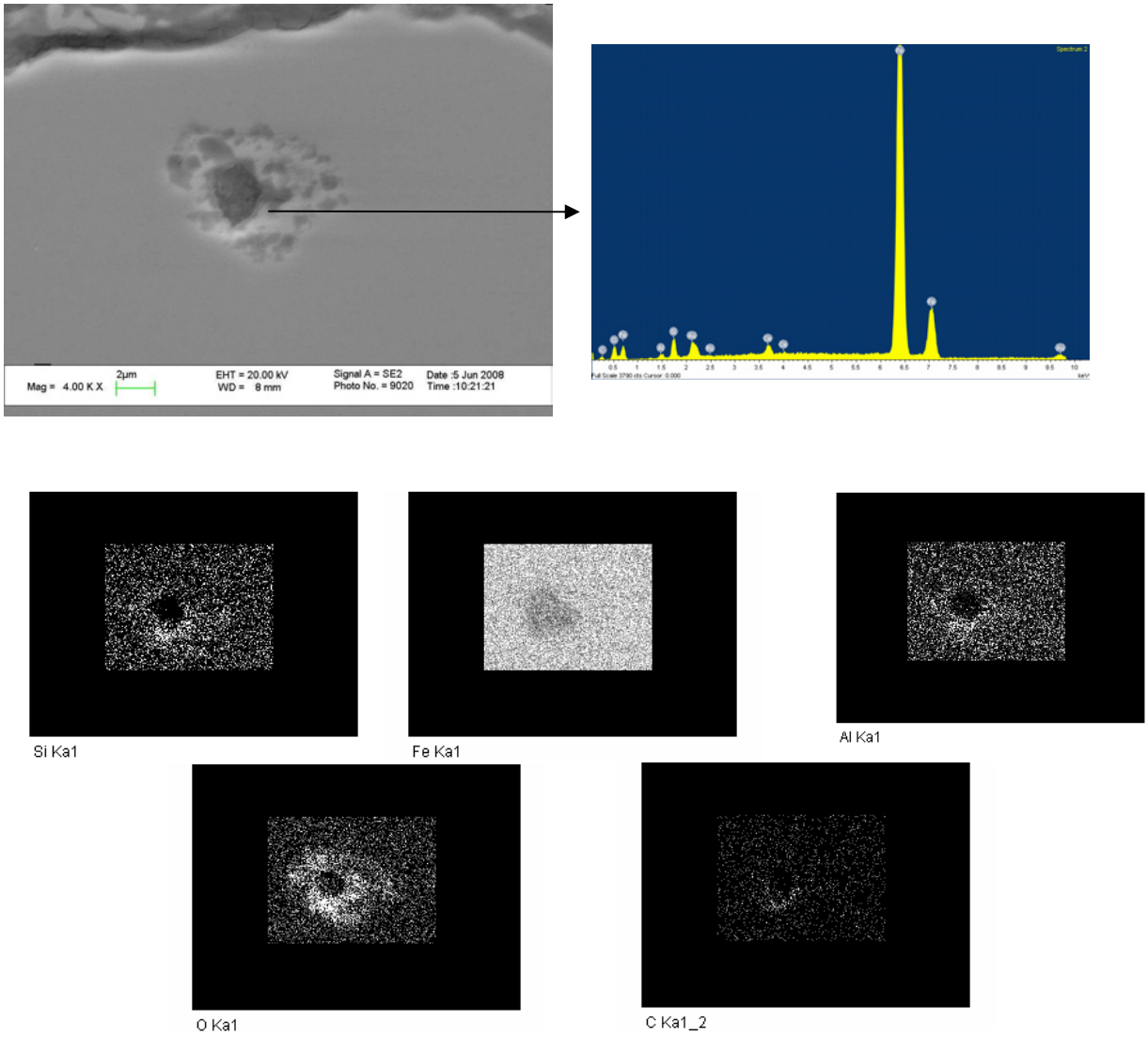

Figure 52 *XRD analysis of internal oxidation of Steel D-1000 sample*

Steel D-1060

Shape

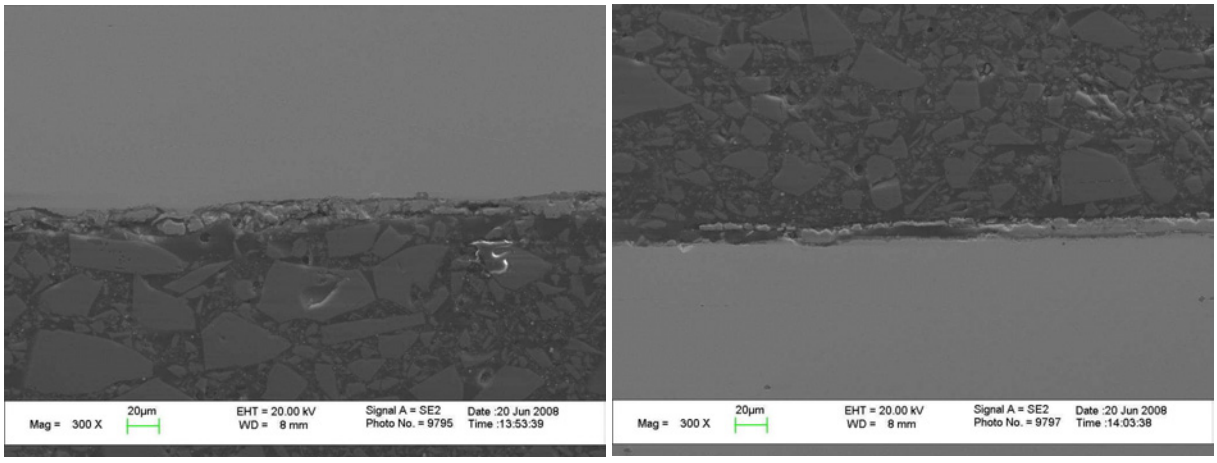

Figure 53 *Steel D-1060 SEM images at 300X*

Composition

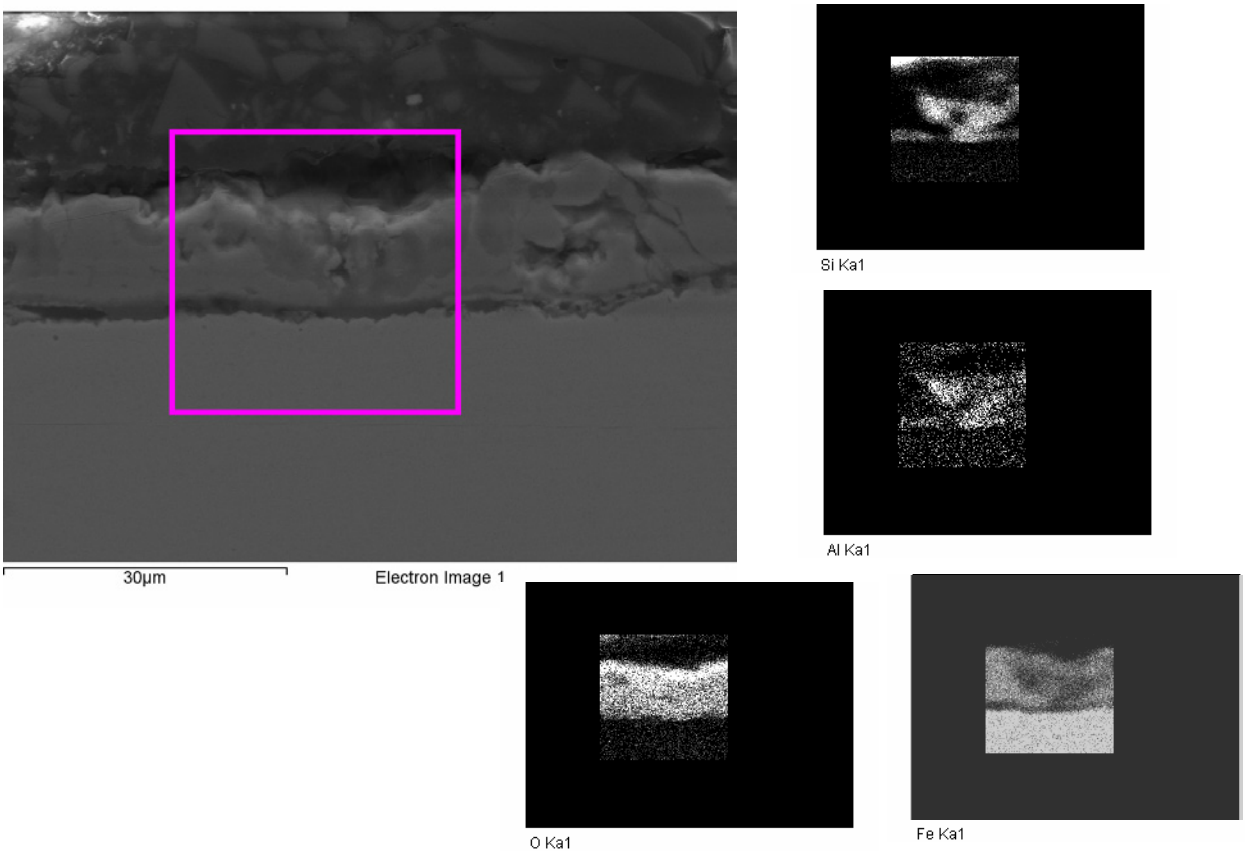

Figure 54 *Steel D-1060 XRD mapping*

Steel B -1000

Shape

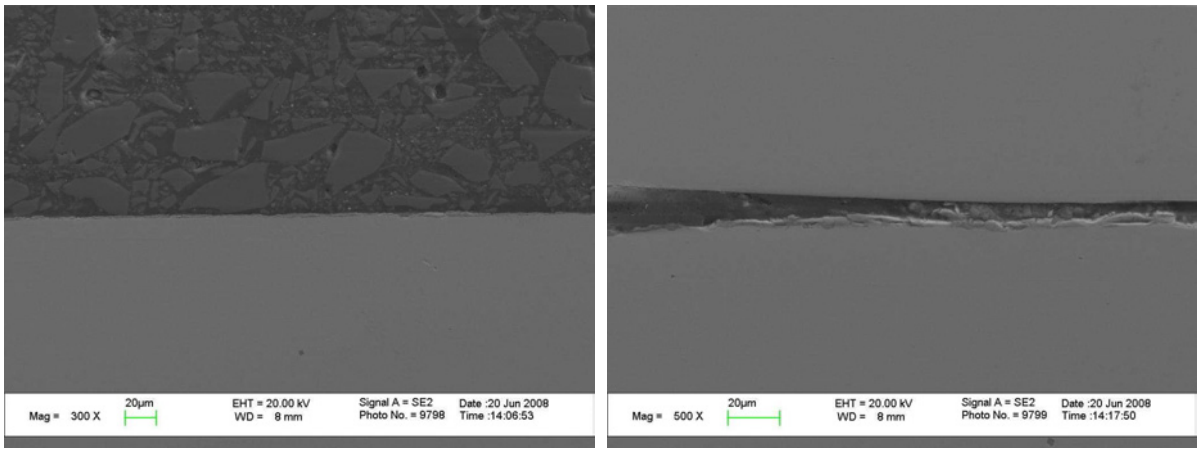

Figure 55 *Steel B-1000 SEM image*

Composition

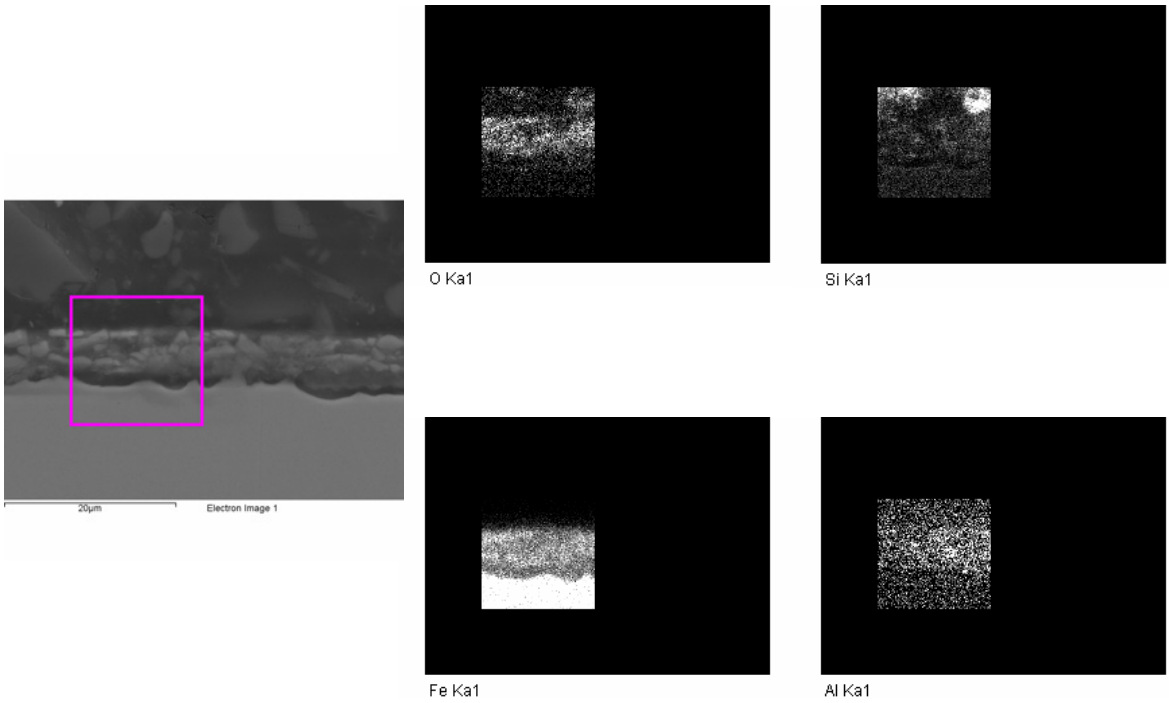

Figure 56 *Steel B-1000 XRD mapping*

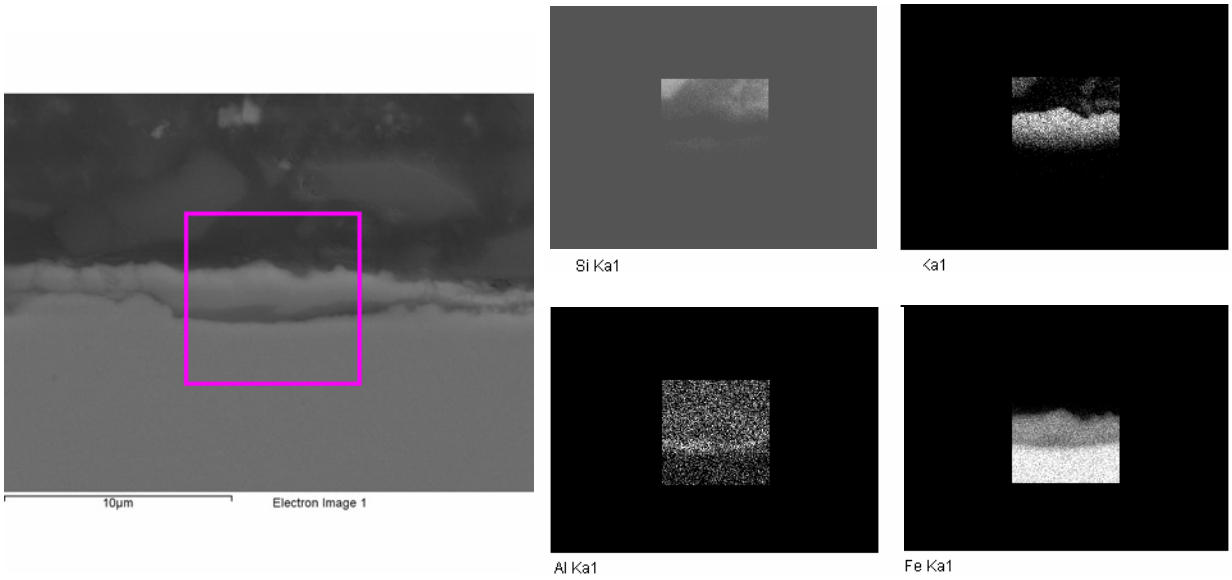

Figure 57 *Steel B-1000 XRD mapping*

Steel B-1060

Shape

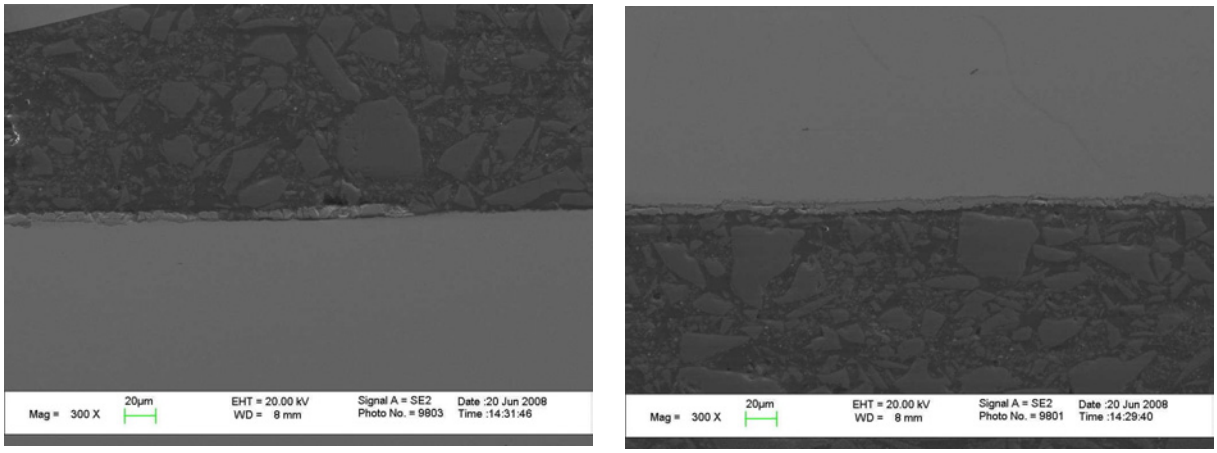

Figure 58 *Steel B-1060 SEM image at 500X*

Composition

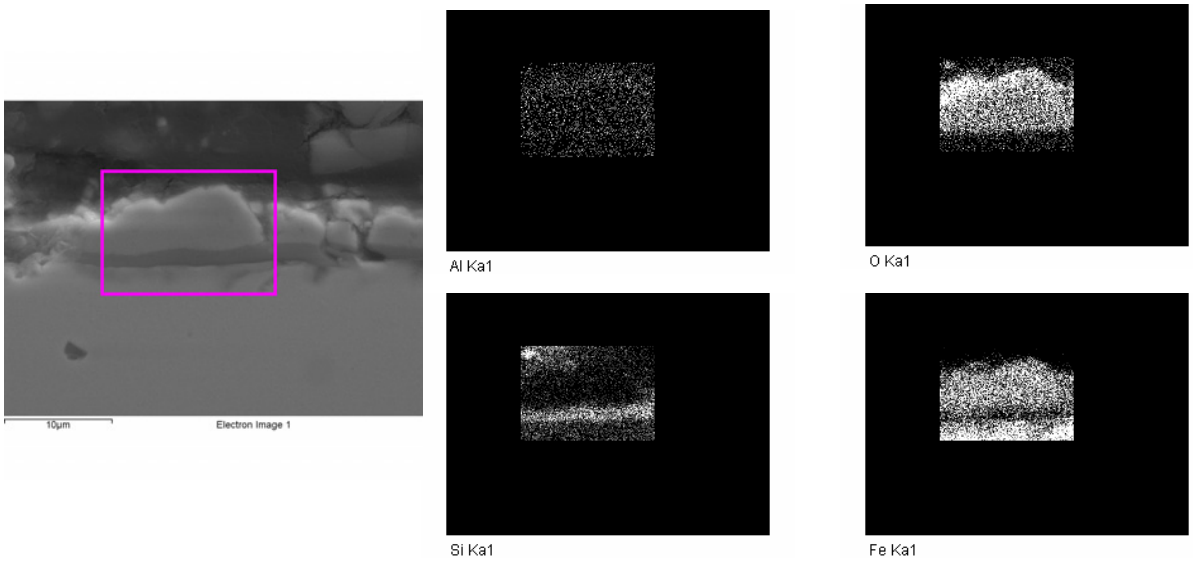

Figure 59 *Steel B-1060 XRD mapping*

The sample thickness of the oxide layer were measured in all the samples, the results are represented in the following graph,

Thickness

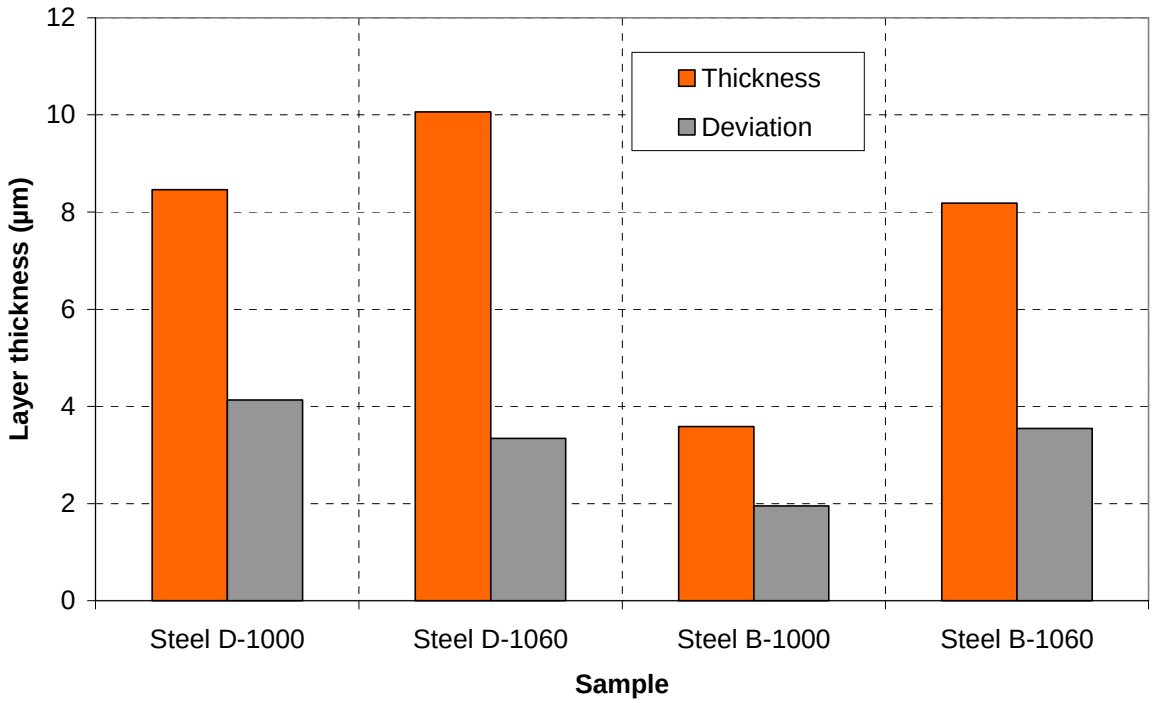

Figure 60 *Thickness of the oxide scales and standard desviation of the measure*

In Fig. 60 it can be seen that the *thickness* of the oxide scale depends on the composition and soaking temperature. Steel D has a thicker oxide scale for all the temperatures than Steel B, and if the soaking temperature is increased the thickness of the oxide scale also augments. In the graph the standard deviation of the measurements is also represented. Steel D at 1000ºC is the layer with the larger deviation, since its thickness is variable, as is shown in Fig. 50. Generally, the Steel B has less variability in the thickness than Steel D as it can be seen in Fig.60, and Figs.55 and 58.

Another important parameter is the *adhesion* of the oxide scale on the sample. The sample with a more adhesive oxide layer is Steel B at 1000º, while in the case of both materials at 1060ºC, the oxide scale has a different adhesion in each side of the sample. In one side the scale is well glued to the sample, while in the other side there is not an uniform scale, since there are parts of the scale that have fall down.

On the other hand, the *composition* of the different samples is also different, see Figs. 51, 54, 56, 57 and 59. Steel D-1000 is constituted by two layers: The first layer is formed by a Si-Al-Fe oxide, while second layer is mainly composed by an iron oxide. Steel D at 1060ºC has the same two layers, but there are also islands of Al-Si-Fe oxides inside the iron oxide. Steel B-1000 has two different kinds of oxide scale compositions, in the first case it has the same two layers of Steel D-1000 and in the second case there is only one layer composed by Al-Si-Fe oxides. Finally, Steel B-1060 has also two layers, but in this case the first layer has not Al element. As previously was shown, the oxides involved

in the scale formation are: FeO, Fe_3O_4, Hercynite ($FeAl_2O_4$), and Fayalite Fe_2SiO_4. Therefore, the Si-Al-Fe oxide is a mixture of Hercynite and Fayalite, while in Steel D-1060 the first layer is only composed by Fayalite.

Internal oxidation was also analyzed. Steel D-1000 presents internal iron oxides, close to the the oxide scale, see Fig. 52.

5 Conclusions

5.1 Influence of Mn, Ni and Cr on a low loss electrical steel

We can conclude that Cr addition has a detrimental effect on the magnetic losses. The increase of magnetic losses with the addition can be due to two reasons: the effect of Cr precipitates or the external oxidation of the samples.

The addition of Ni element seems to decrease the magnetic losses. Moreover, it also has an effect on texture, since it appears to inhibit γ fibre. This development on texture appears to be the origin of the improvement on magnetic properties, since grain size has not a trend that can explain this improvement.

Finally, magnetic losses and grain size seems to remain constant when Mn content is increased. On the other hand, the variation of the texture factor is not regular, in fact the study of the homogeneity done on the sample of low Mn reveals that the texture is not homogeneous along the sample. It is also important to consider the final mechanical properties, since for elevate Mn contents appears cracks in the middle of the samples that can reduce the workability and deteriorate the magnetic properties.

Note that the reproducibility of the experiment is limited by the variation of the other alloying contents and process parameters; hence it would be interesting to perform new experiments adding a larger range of Ni and Cr content, and controlling the variation of the rest of alloying elements and processing parameters.

Further work is required on the optimization of laboratory processing in order to obtain more homogeneous materials. In addition, additional work must be done in order to understand the apparent beneficial effect of Ni on the texture and magnetic properties of steel and to discern what the real influence of Mn on them is.

5.2 Effect of soaking temperature on the magnetic properties and grain size of electrical steels with different chemistries

Magnetic losses decrease when the soaking temperature is increased for low temperatures, but it achieves a minimum on magnetic looses that varies depending on the material. In the case of Steel B (Si+Al=3.3%) the minimum is in the range 1040-1060ºC, Steel A (Si+Al=2.8%) is in the range 1040-1080ºC and SteelC (Si+Al=3.8%) in the range 1020-1060ºC.. In the case of Steel D (Si+Al=4.2%) it is the amount of experimental data does not allow to determine where the minimum for the loss is. Soaking temperature also affects the grain growth of the material. The higher the soaking temperature, the coarser the final grains. It has been modelled the grain growth as a function of the temperature for Steel A, Steel B and Steel C. On the other hand, when the magnetic losses are represented as a function of the grain size, all the materials present a minimum in total looses around 90-130µm.

The study of the oxidation scale reveals that the composition, thickness and adhesion of the layer depend on the composition of the samples and the soaking temperature. Generally, the higher is the soaking temperature the thicker is the oxide scale. Steel D (Si+Al=4.2%) material has a thicker scale than Steel B (3.8%) for all temperatures. The sample with a more adhesive oxide layer is Steel D at 1000º, while in the case of both materials at 1060ºC, the oxide scale have a different adhesion in each

side of the sample. In one side the scale is well glue to the sample, while in the other side there is not an uniform scale, since there are parts of the scale that have fall down. Another important parameter is the internal oxidation, since Steel D-1000 presents internal iron oxides, close to the oxide scale.

Finally, there is also variation on the composition since in Steel D material always has a mixture of iron oxides and Hercynite ($FeAl_2O_4$), and Fayalite (Fe_2SiO_4). While in the case of Steel B when it is applied a temperature of 1060ºC the Hercynite layer does not appear, so it is a mixture of iron oxides and Fayalite.

6 Bibliographic references

[1] José Barros Lorenzo, Production of Si-Steel by Hot Dipping and Diffusion annealing, *Faculteit Ingenieurswetenschappen* (2006-2007).

[2] Monika Jenko, Blazenko Korousic, Djordje Mandrino, Vasilij Presern, HRAES study of oxide scale formation by decarburization of non-oriented electrical steel sheets, *Vacuum*, 57, 295-305 (2000).

[3] Lucía Suárez Fernández, Growth and Deformation Behavior of Oxide Scale on Steel, *Faculteit Ingenieruswetenschappen* (2007-2008).

[4] K.Numakura, A. Tsugawa, M. Sugano, and Y. Sato, Magnetic and electrical properties of Iron-Silicon alloys, *Science Reports of the Imperial Univ. of Tohoky*, 24(1-2) (1972).

[5] W.E.Ruder, *U.S. Patent 1*, 110 010 (1912).

[6] M.Shioki and Y.Kurosaki, The Effects of Grain Size on the Magnetic Properties of Nonoriented Electrical Steel Sheets, *J. Materials Engineering*, 11 (1), 37 (1989).

[7] R. Bozorth, Ferromagnetism, *John Wiley-IEEE* (2003).

[8] H. Williams, Magnetic properties of single crystals of silicon-iron, *Physical Review*, 52, 747-751 (1937).

[9] Jong T.Park, Jong S.Woo and Sam K.Chang, Effect of soaking temperature and annealing atmosphere on magnetic properties of semi-processed nonoriented electrical steel containing 0.4%Silicon, *Steel research*, 69 (2) (1998).

[10] C.K.Hou and P.C.Wang, Effects of composition and process variables on core loss and hardness of low carbon electrical steels, *Journal of Magnetism and Magnetic Materials*, 92, 109-115 (1990).

[11] Marco A, da Cunha and Sebastiao C, Paolinelli, Effect of Hot Rolling Temperature on the Structure and Magnetic Properties of High Permeability Non-oriented Silicon steel, *Steel research*, 76 (6) (2005).

[12] P.K Rastogi, Effect of Chromium on the magnetic properties and texture of non-oriented steel, *Journal of Magnetism and Magnetic Materials* (1975).

[13] K. Jenkins, M. Lindenmo, Precipitates in electrical steels, *Journal of Magnetism and Magnetic Materials* (2004).

[14] K. Günter, F. Böling, Detrimal effect of oxidation on magnetic properties of nonoriented electrical steel sheets, *J. Applied Phys.*, 64 (1998).

[15] R. Kay J. J. Jonas Mp. Butronguillen and J.Savoie, Transf ormation Textures in Steels, *ISIJ International*, 34 (12), 927-942 (1994).

[16] Alberto Monsalve G., Descripción de texturas por medio de la función de distribución de orientaciones, *Simposio materia* (2003).

[17] H. J. Bunge, Texture analysis in Material science, Mathematical methods, *Butterwords* (1982).

[18] Yan Bo CAI and Sam Kyu CHANG, Effect of Two-step Annealing on Texture and Magnetic Properties by Addition of Co, Mo, or ni in Silicon steel, *ISIJ International*, 47 (11), 1680-1686 (2007).

[19] Hyroyoshi YASHIKI and Teruo KANEKO, Effects of Mn and S on the Grain Growth and Texture in Cold Rolled 0.5% Si Steel, *ISIJ International*, 30 (4) (1990).

[20] Kenji Narita and Masato Enokizono, Effect of Nickel and Manganese Addition on Ductility and Magnetic properties of 6.5% Silicon-Iron Alloy, *IEEE Transactions on Magnetics*, 14 (4) (1978).

[21] R.F.Cardoso, L. Brandao, M.A, Cunha, Influence of Grain Size and Additions of Al And Mn on The Magnetic Properties of Non-oriented Electrical Steels With 3 wt.%Si, *Materials Reserachs*, 11 (1), 51-55 (2008).

7 Appendix

7.1 Measured data for Mn, Ni and Cr addition samples

Sample	P15(W/Kg)	Standard deviation	$P15_{Hys}$(W/Kg)	Standard deviation	Main diameter(μm)	Standard deviation
B109A	2.61	0.13	1.81	0.05	135.99	19.90
B110A	2.46	0.11	1.61	0.06	225.53	64.77
B111A	2.45	0.09	1.65	0.04	153.39	15.44
B112A	2.40	0.03	1.59	0.05	111.65	8.33
B113A	2.90	0.09	1.94	0.07	145.40	36.47
B114A	2.57	0.05	1.72	0.02	149.68	27.77
B115A	2.54	0.10	1.76	0.07	94.83	4.23
B116A	2.58	0.17	1.82	0.10	88.53	9.90
B117A	3.11	0.21	2.33	0.22	124.86	6.41

Table 8 *Data for Group A of Mn Ni and Cr addition samples*

Sample	P15(W/Kg)	Standard deviation	$P15_{Hys}$(W/Kg)	Standard deviation	Main diameter(μm)	Standard deviation
B109B	2.65	0.13	1.76	0.06	173.02	20.31
B110B	2.81	0.12	1.99	0.06	144.16	22.20
B111B	2.73	0.06	1.96	0.05	175.75	24.22
B112B	2.63	0.08	1.91	0.06	113.67	13.42
B113B	2.37	0.04	1.46	0.08	176.76	30.97
B114B	2.30	0.05	1.45	0.05	163.57	31.36
B115B	2.50	0.04	1.77	0.03	110.90	17.67
B116B	2.87	0.11	2.15	0.08	112.68	40.35
B117B	3.26	0.17	2.43	0.15	158.00	43.68

Table 9 *Data for Group B of Mn Ni and Cr addition samples*

7.2 Experimental Gleeble test

A letter has been designed for each material in order to facilitate the notation.

Steel A cycles (groupL)

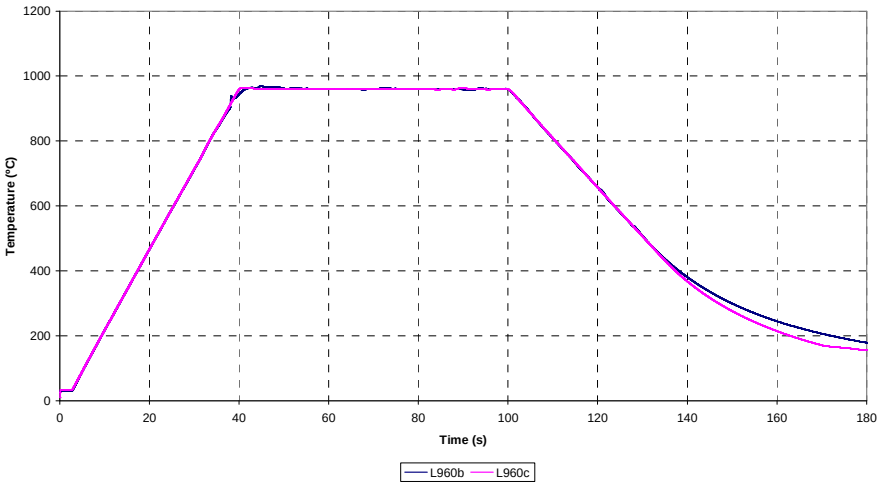

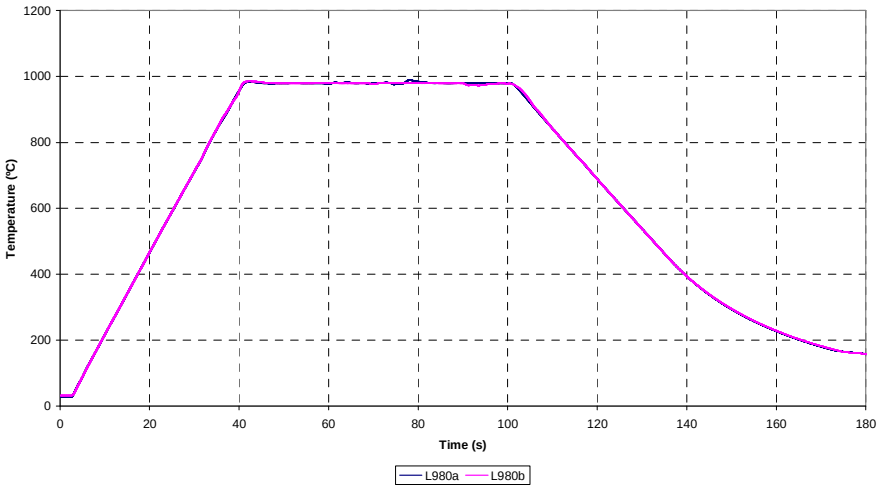

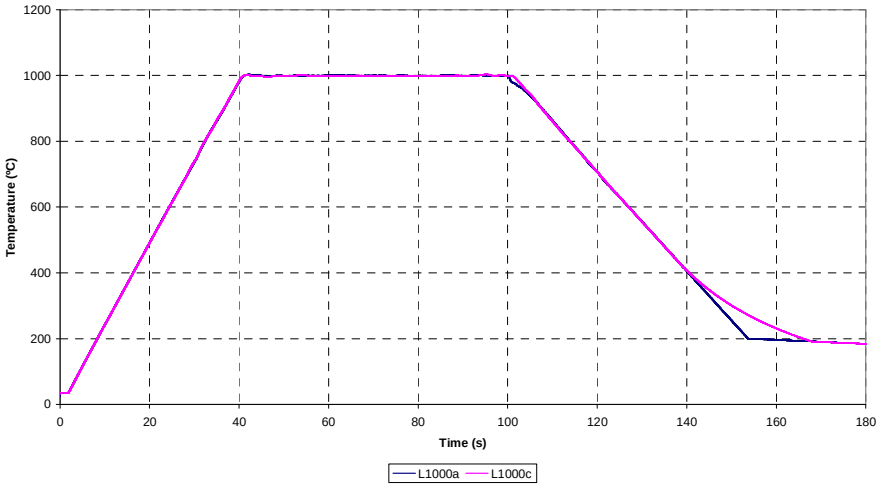

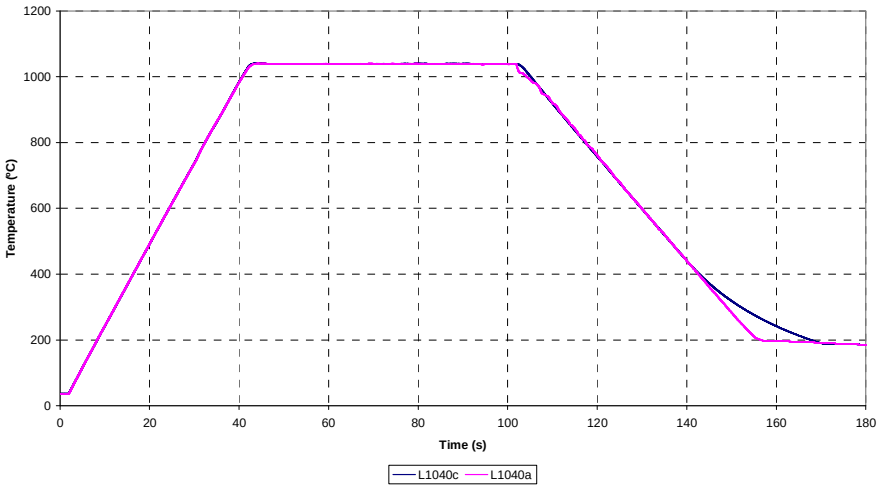
Temperature (°C)
Time (s)
L1040c
L1040a

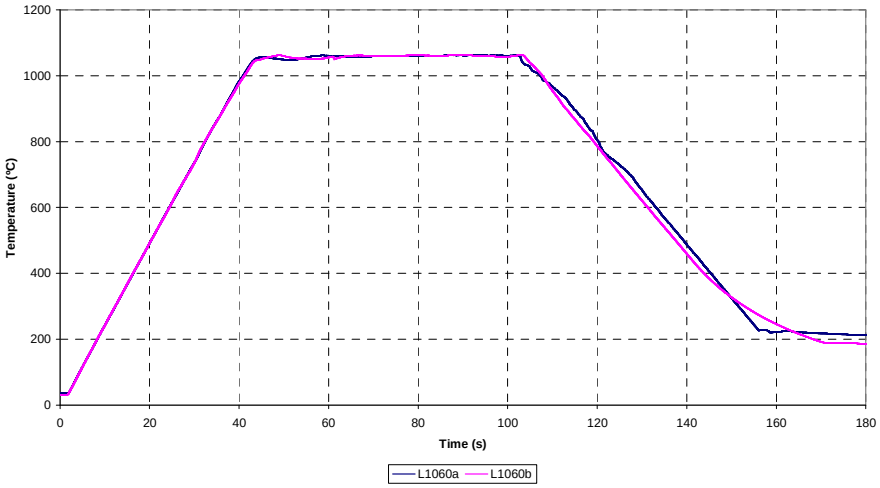
Temperature (°C)
Time (s)
L1060a
L1060b

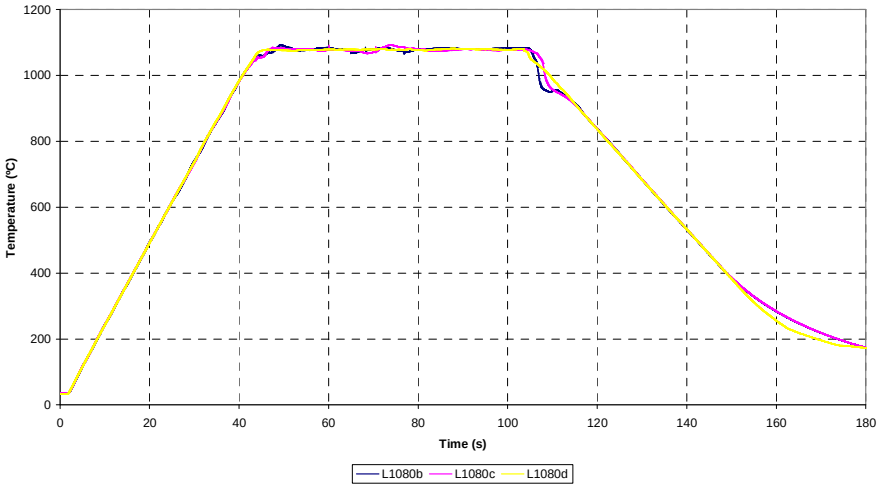
Temperature (°C)
Time (s)
L1080b
L1080c
L1080d

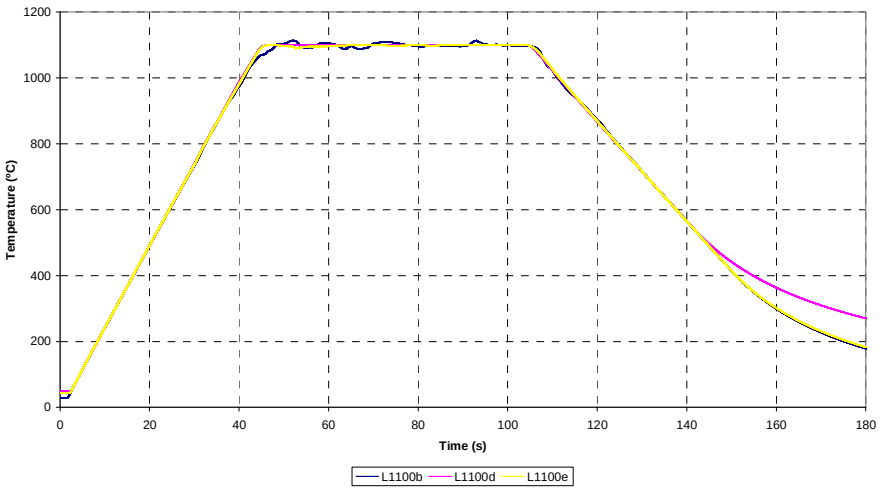

Steel B cycles(GroupJ)

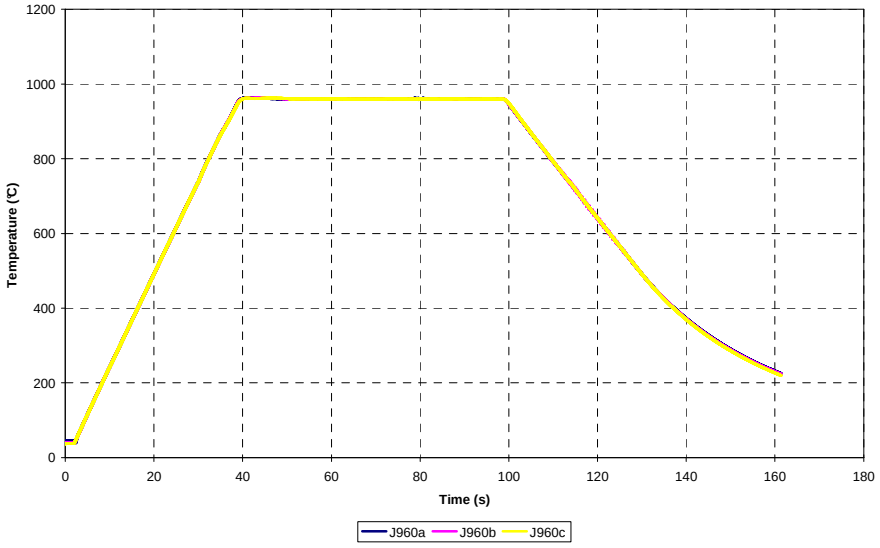

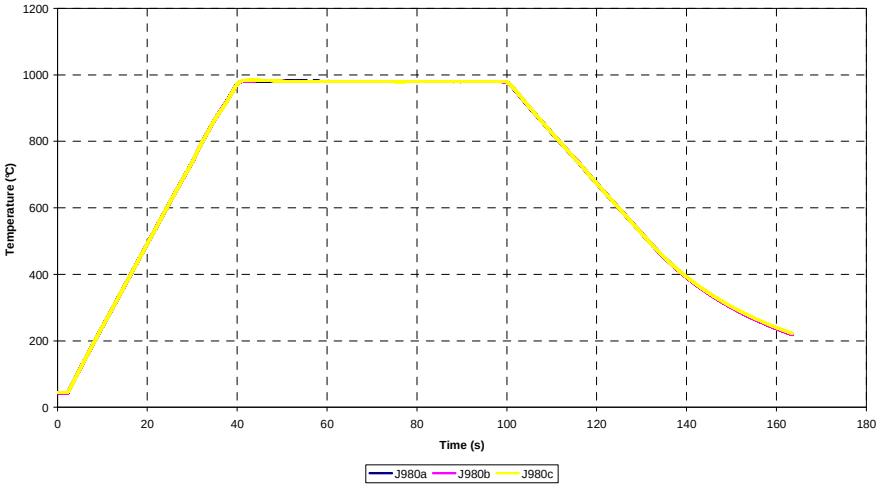

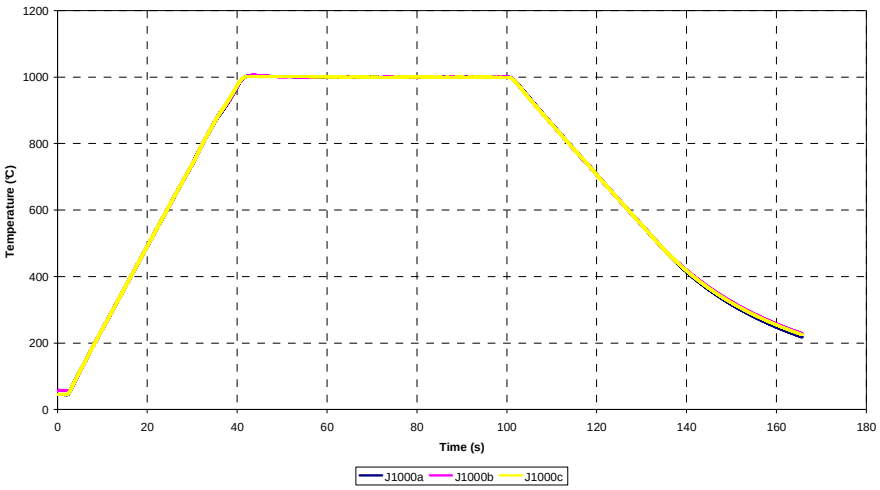
Temperature (ºC)
Time (s)
J1000a
J1000b
J1000c

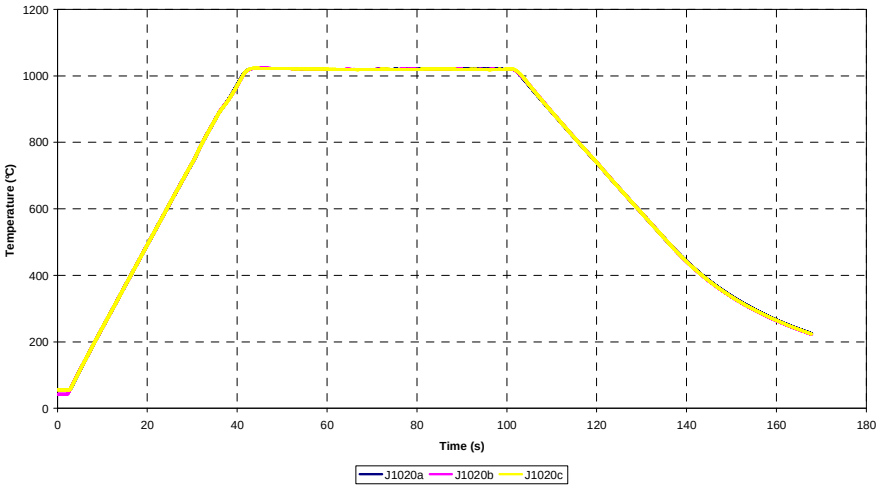
Temperature (ºC)
Time (s)
J1020a
J1020b
J1020c

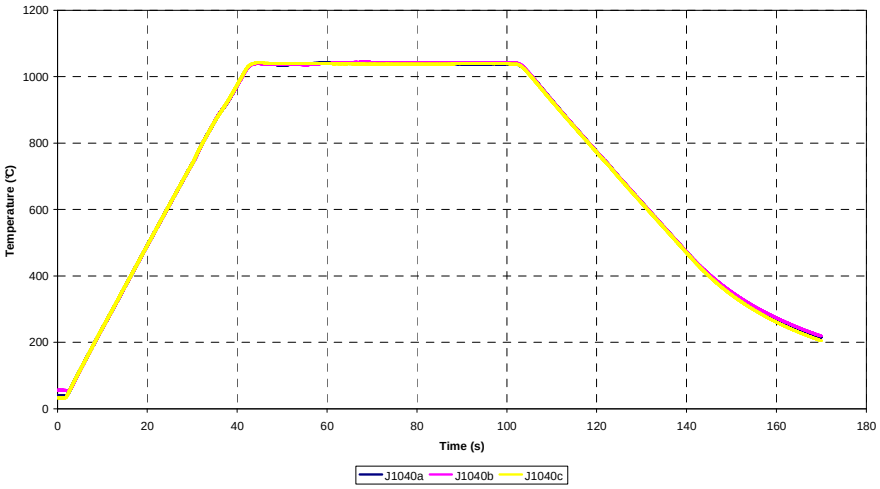
Temperature (ºC)
Time (s)
J1040a
J1040b
J1040c

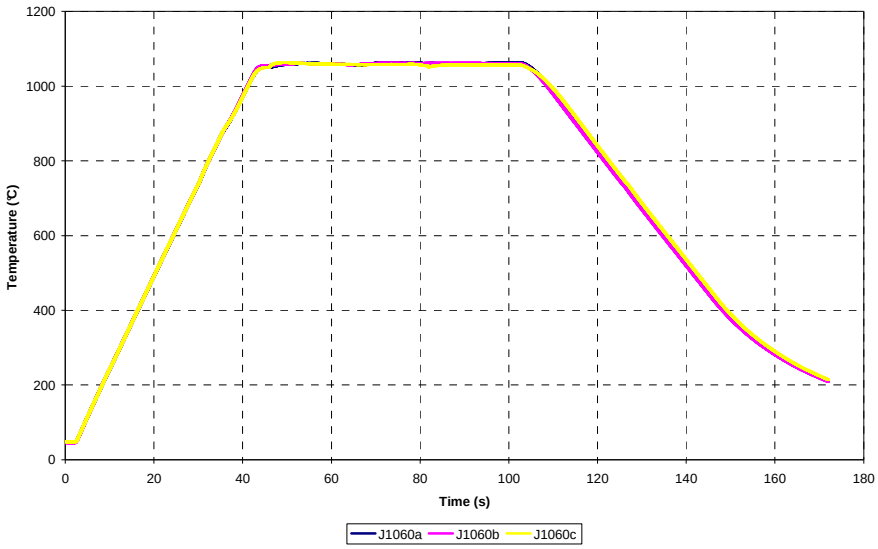
Temperature (ºC)
Time (s)
J1060a
J1060b
J1060c

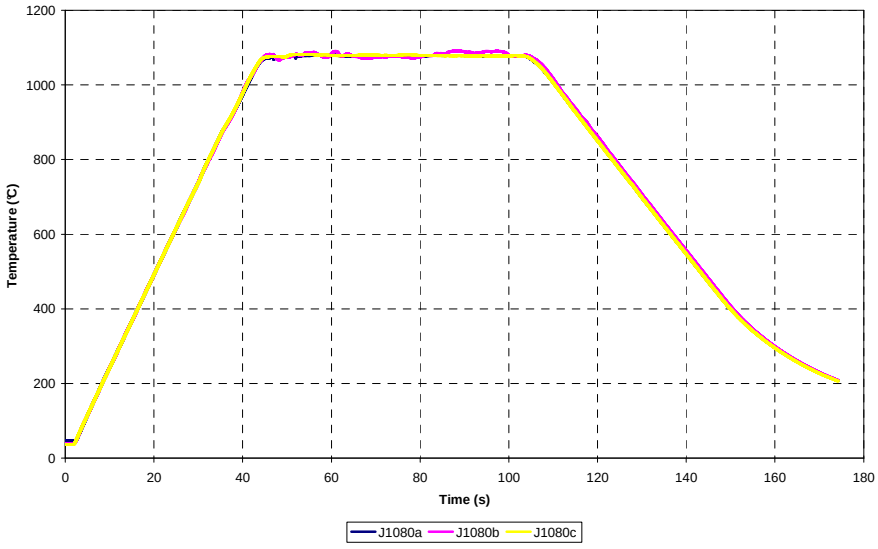
Temperature (ºC)
Time (s)
J1080a
J1080b
J1080c

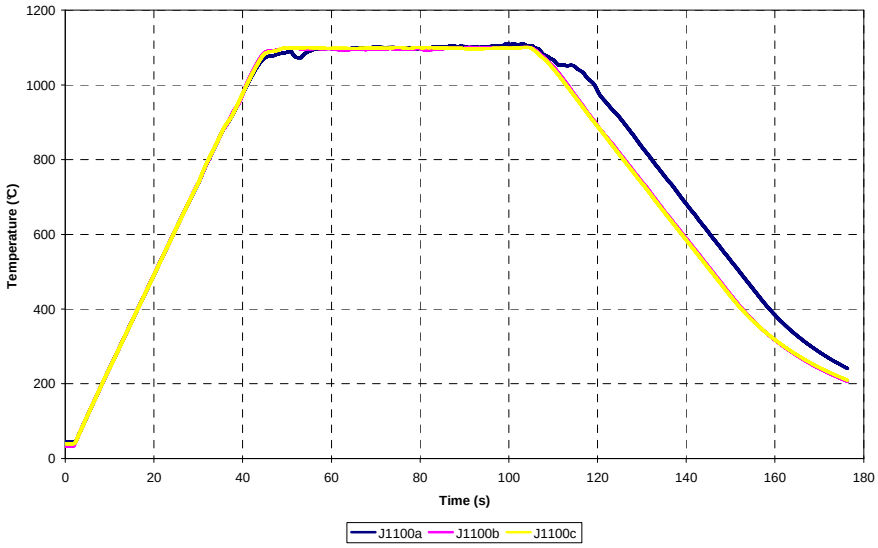
Temperature (ºC)
Time (s)
J1100a
J1100b
J1100c

Steel C cycles (GroupK)

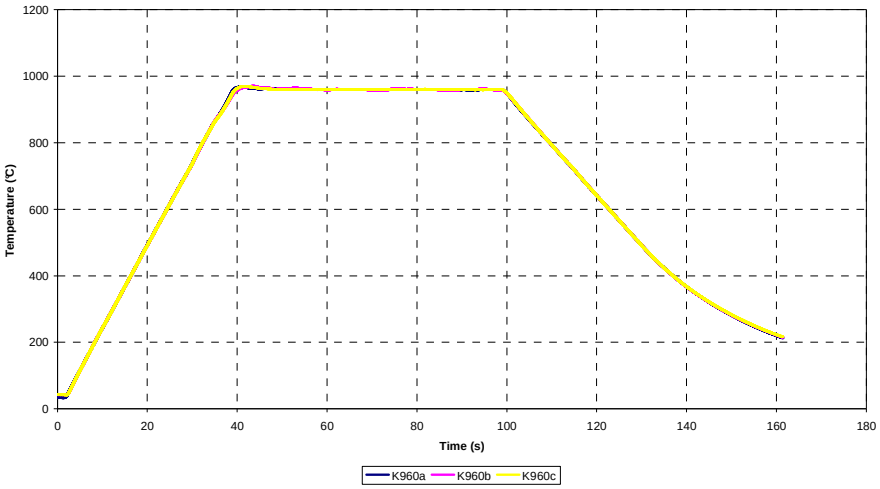

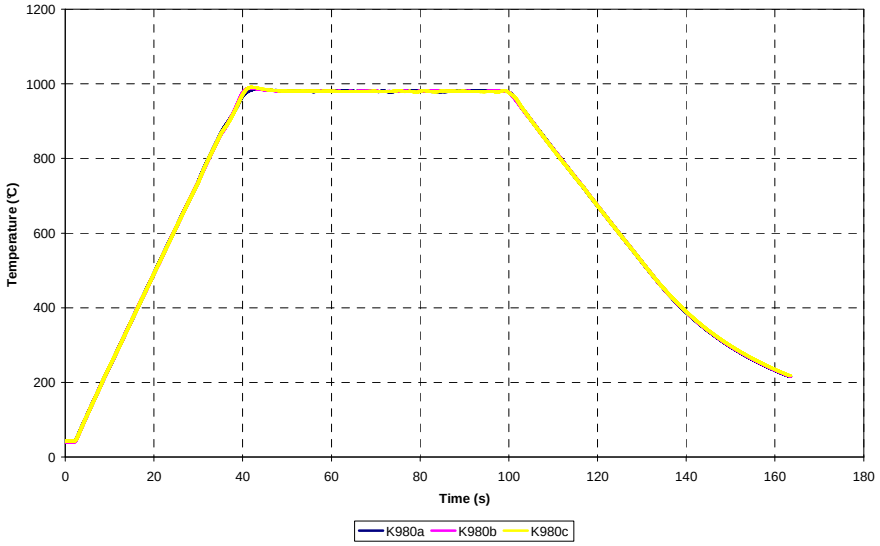

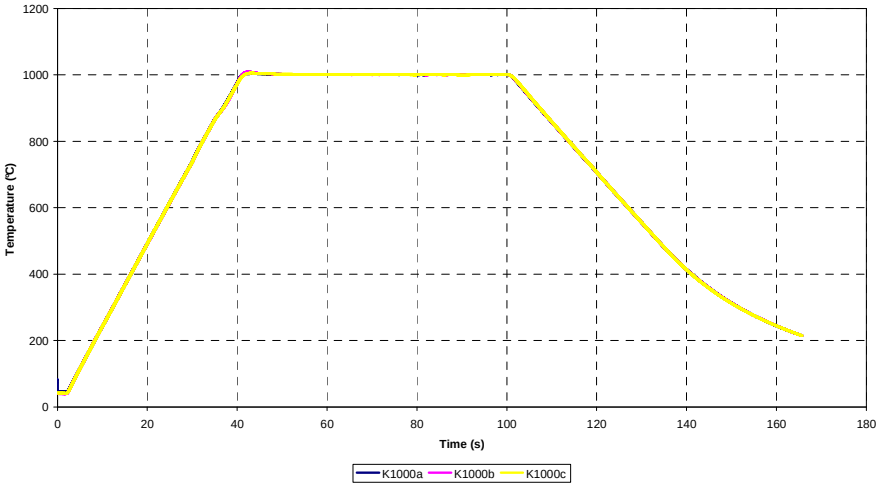

Group K

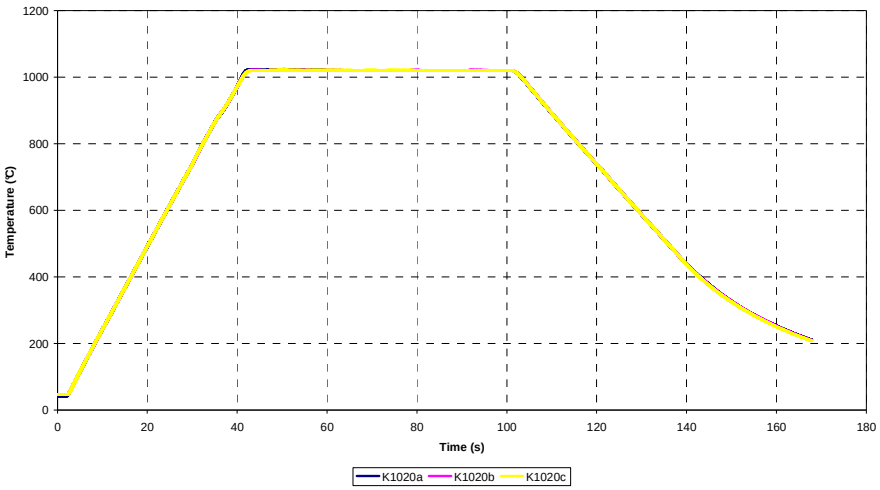
Temperature (°C)
Time (s)
K1020a
K1020b
K1020c

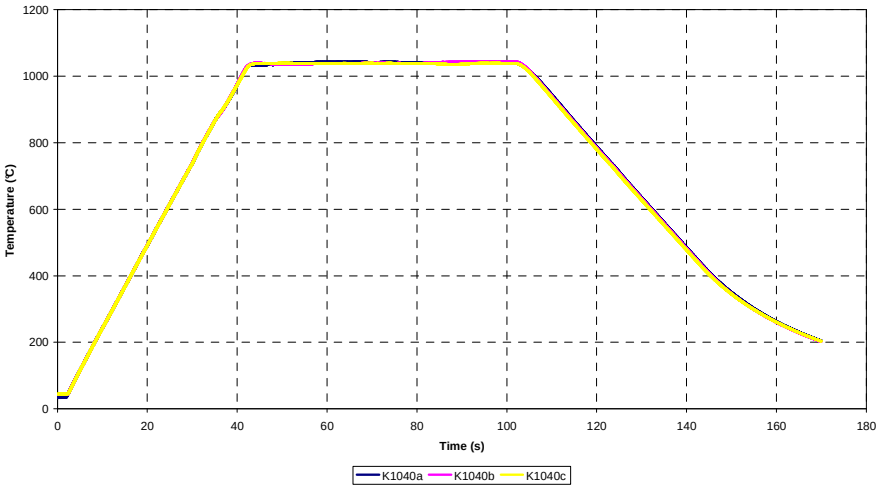
Temperature (°C)
Time (s)
K1040a
K1040b
K1040c

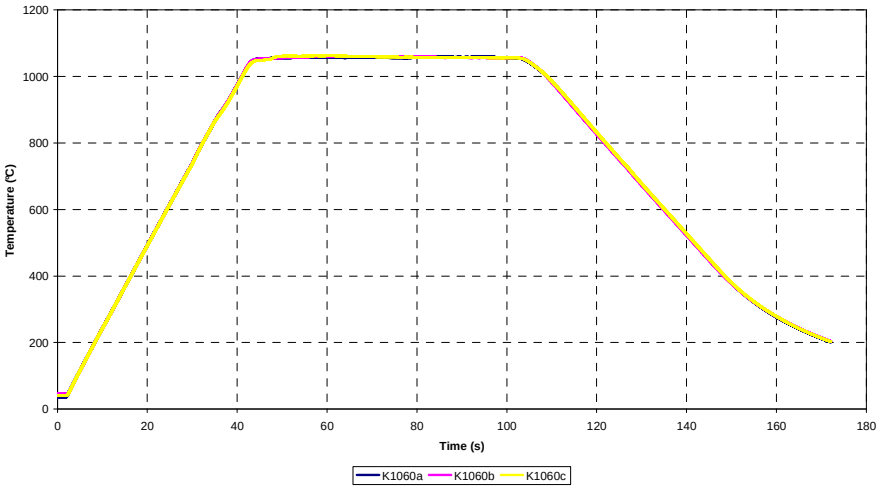
Temperature (°C)
Time (s)
K1060a
K1060b
K1060c

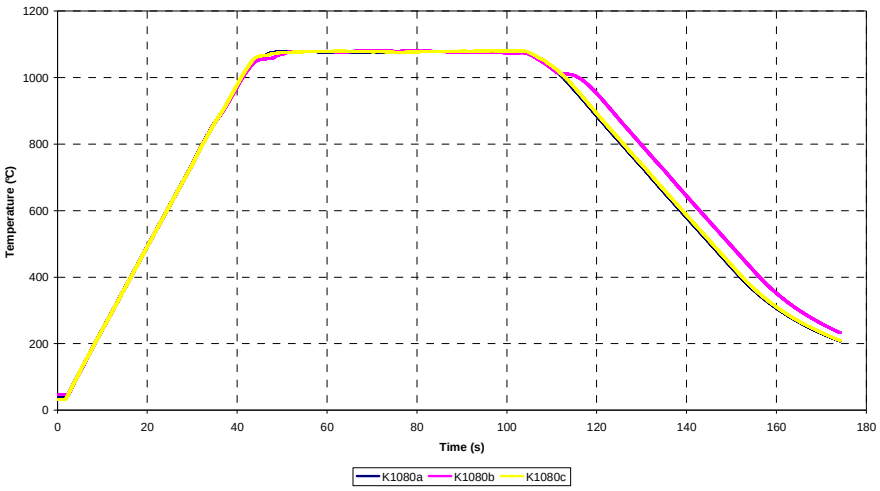

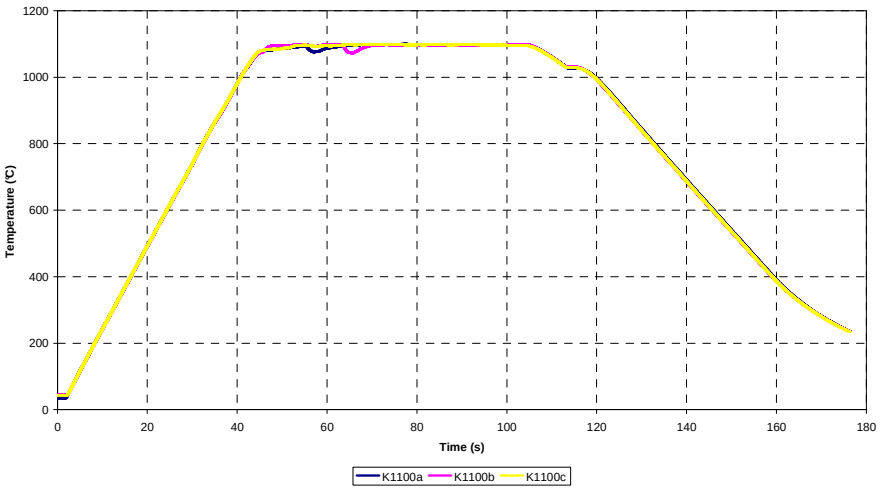

Steel D cycles (Group I)

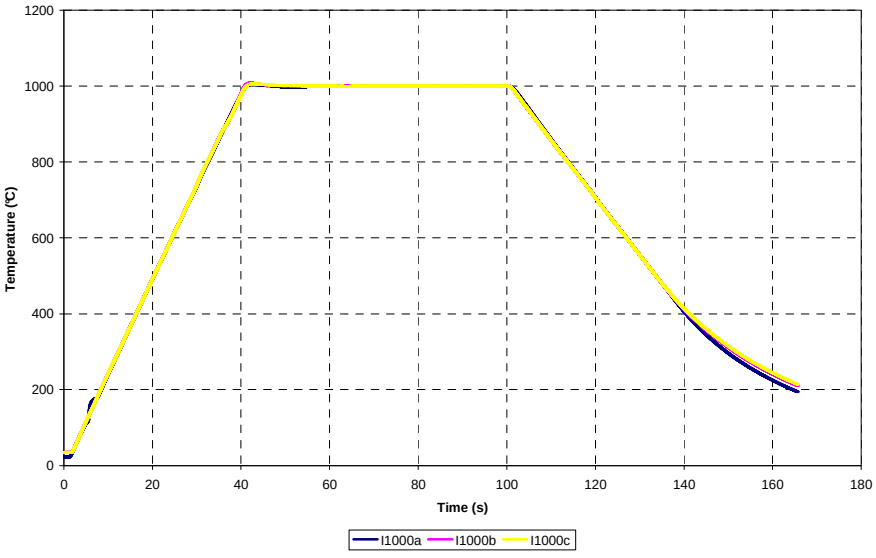

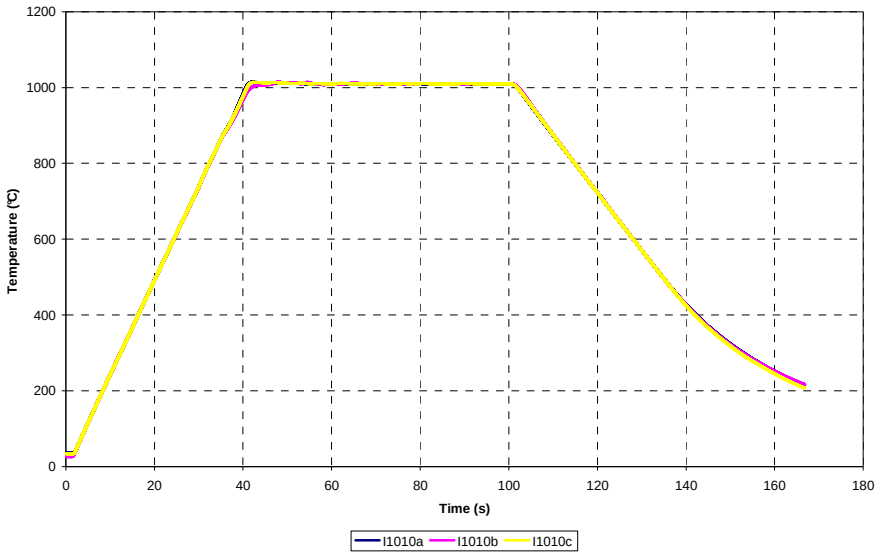
Temperature (ºC)
Time (s)
I1010a
I1010b
I1010c

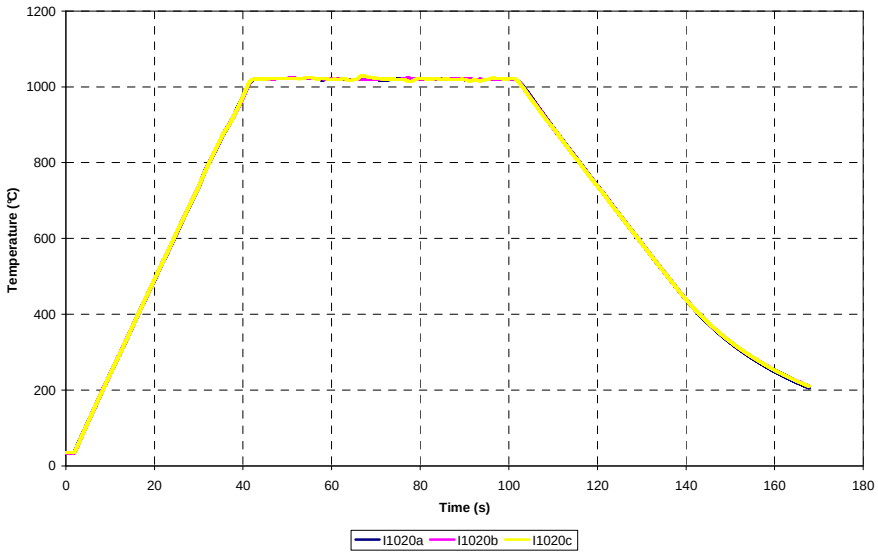
Temperature (ºC)
Time (s)
I1020a
I1020b
I1020c

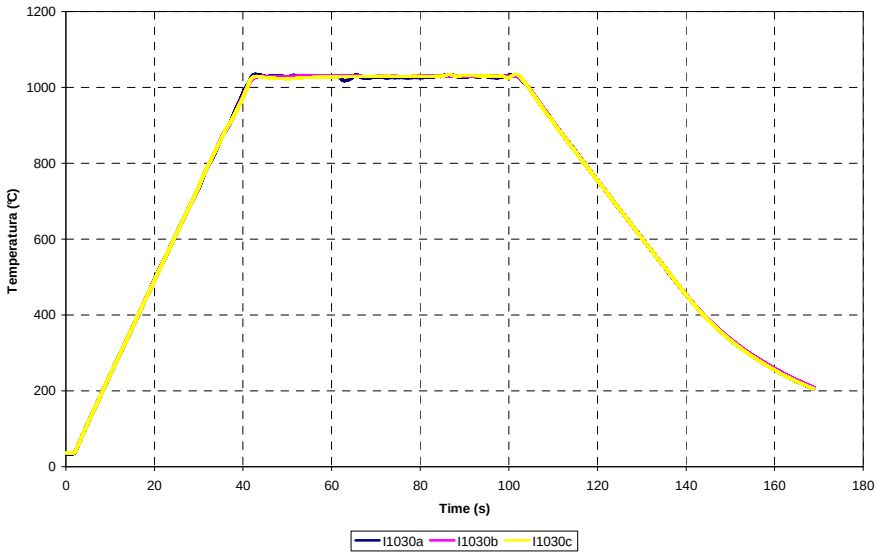
Temperatura (ºC)
Time (s)
I1030a
I1030b
I1030c

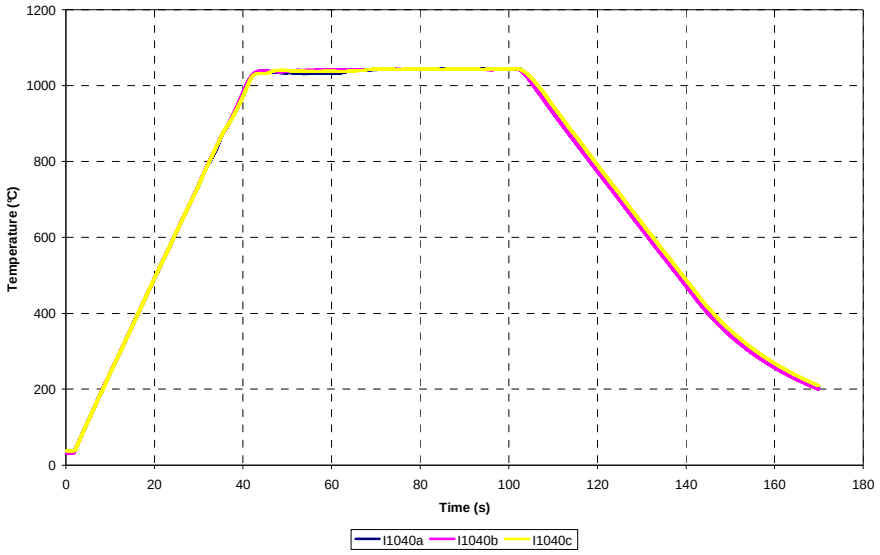
Temperature (ºC)
Time (s)
I1040a
I1040b
I1040c

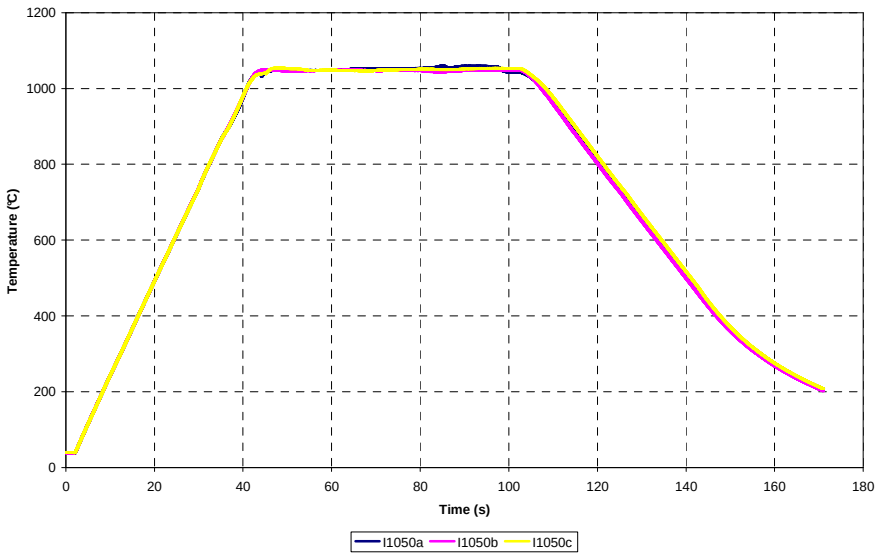
Temperature (ºC)
Time (s)
I1050a
I1050b
I1050c

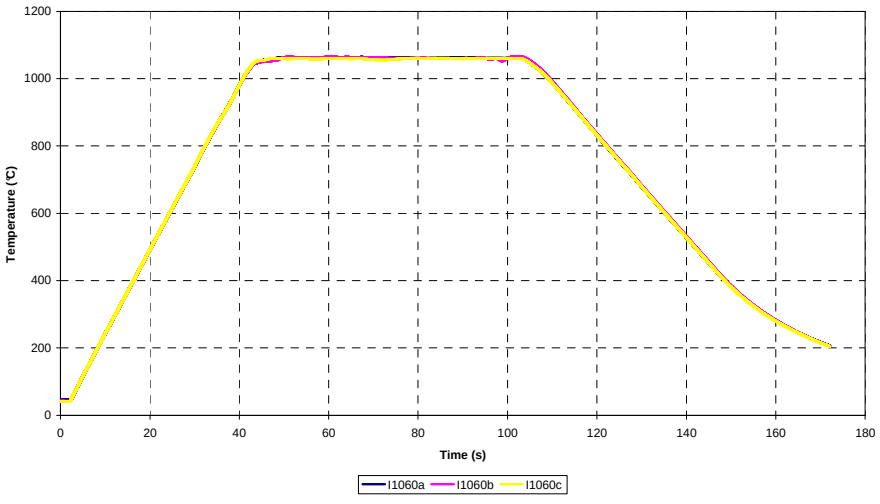
Temperature (ºC)
Time (s)
I1060a
I1060b
I1060c

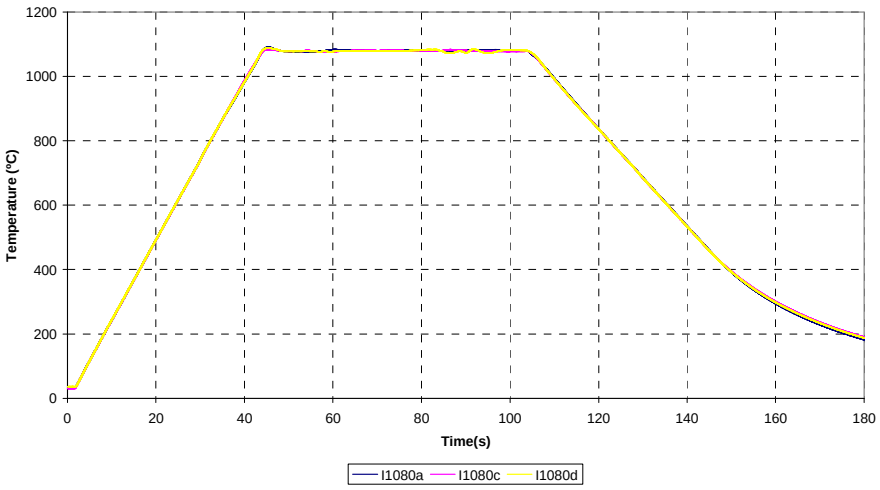
Temperature (ºC)
Time(s)
I1080a
I1080c
I1080d

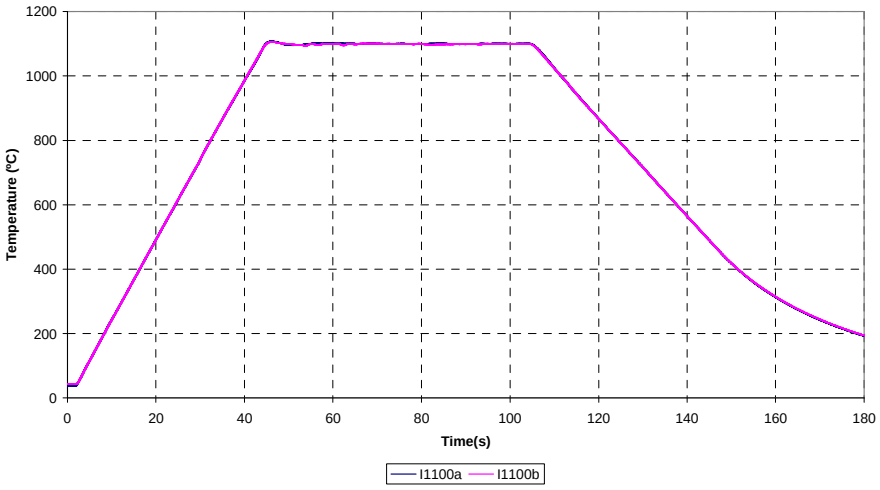
Temperature (ºC)
Time(s)
I1100a
I1100b

7.3 Data obtained after Gleeble tests

Sample	Microstructure	Main diameter (μm)	Standard deviation	P15/50 (W/Kg)	Standard deviation
L960	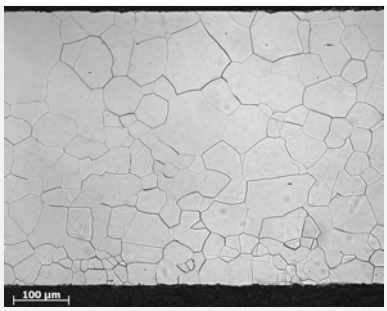	43,50	5,71	3,47	0,14
L980	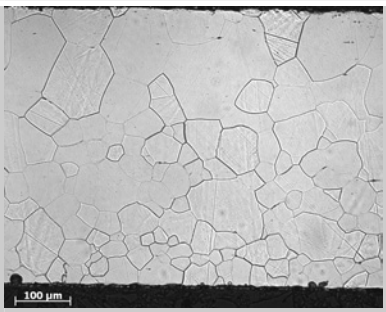	55,25	8,14	3,36	0,07
L1000	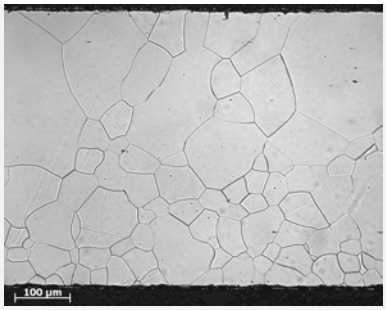	64,08	9,60	3,24	0,04
L1020	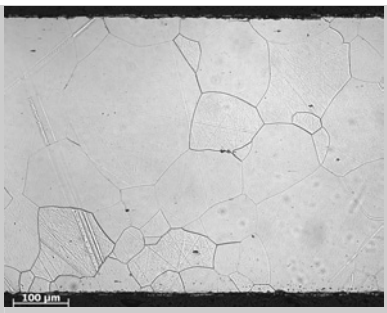	89,75	16,26	3,21	0,12

L1040	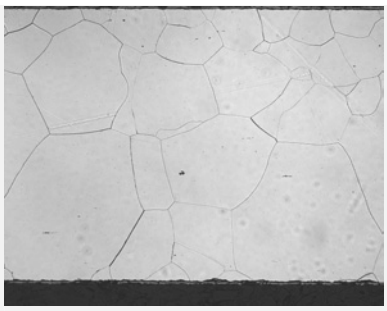	101,49	28,34	3,16	0,12
L1060	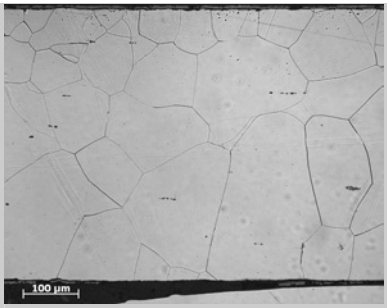	113,56	24,34	3,15	0,06
L1080	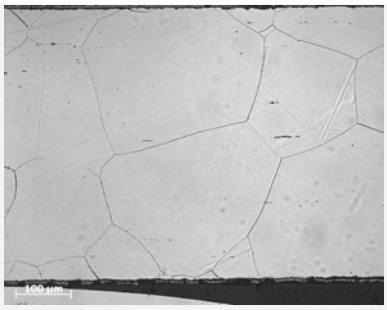	143,30	23,87	3,14	0,09
L1100	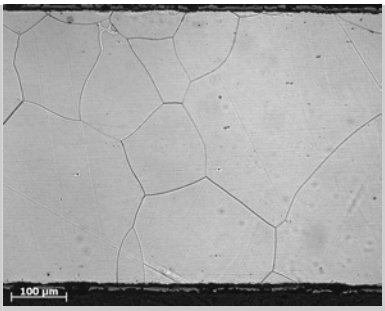	180,86	31,41	3,16	0,14

Table 10 *Data obtained for Steel A*

Sample	Microstructure	Main diameter (µm)	Standard deviation	P15/50 (W/Kg)	Standard deviation
J960	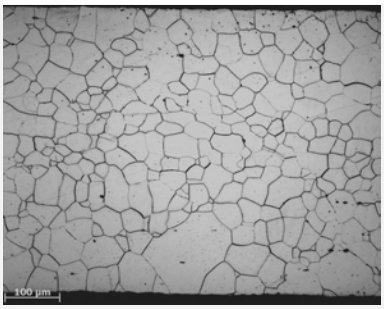	35,74	1,60	3,69	0,13
J980	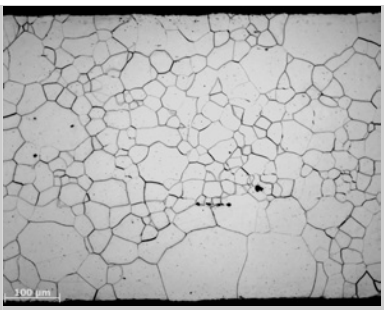	38,42	8,96	3,64	0,12
J1000	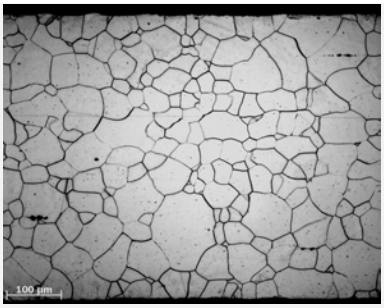	42,80	6,70	3,41	0,11
J1020	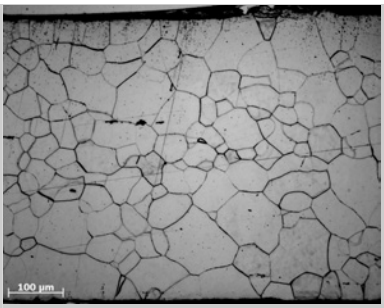	55,79	13,11	3,39	0,09
J1040		66,82	9,63	3,11	0,05

J1060	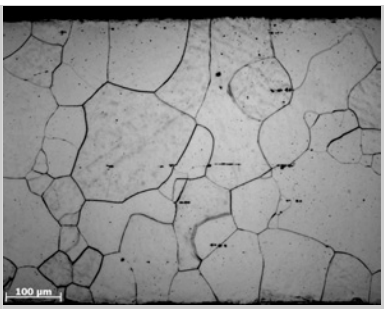	94,91	7,44	3,10	0,09
J1080	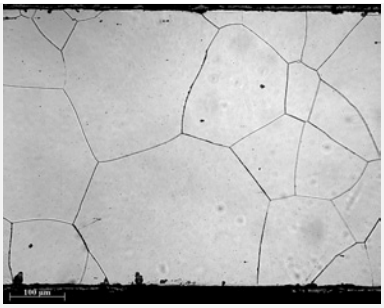	123,65	29,84	3,13	0,07
J1100		149,88	22,77	3,19	0,05

Table 11 *Data obtained for Steel B*

Sample	Microstructure	Main diameter (µm)	Standard deviation	P15/50 (W/Kg)	Standard deviation
K960	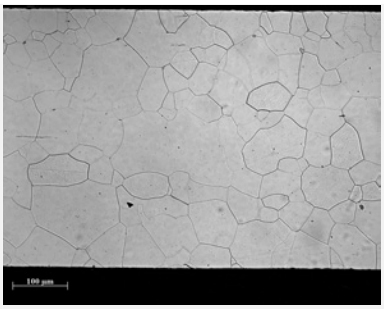	50,47	4,63	2,95	0,09
K980	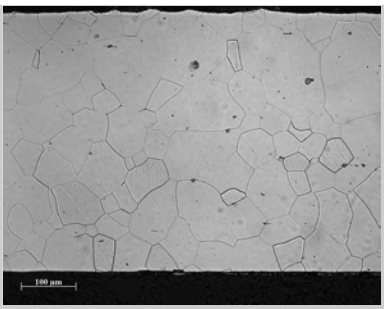	56,96	6,41	2,81	0,09
K1000	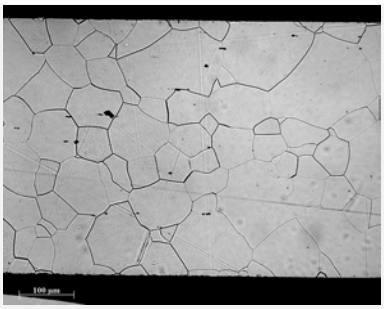	78,00	9,00	2,64	0,02
K1020	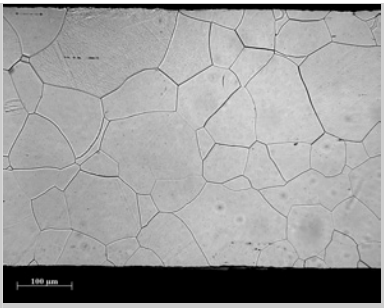	86,55	8,29	2,66	0,05
K1040	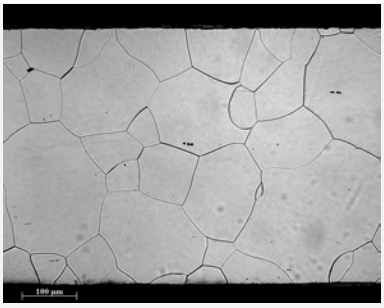	100,17	15,18	2,65	0,03

K1060	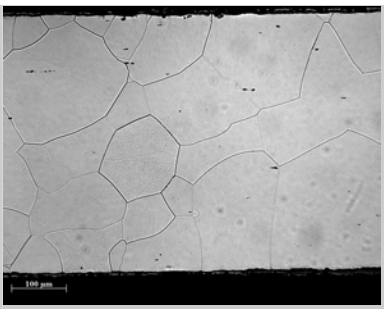	125,06	15,07	2,57	0,07
K1080	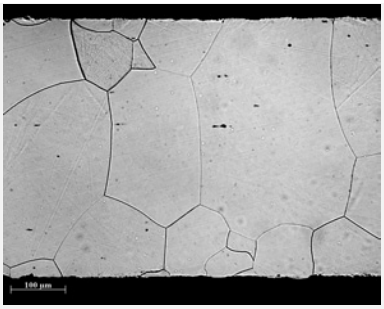	165,42	33,58	2,69	0,08
K1100	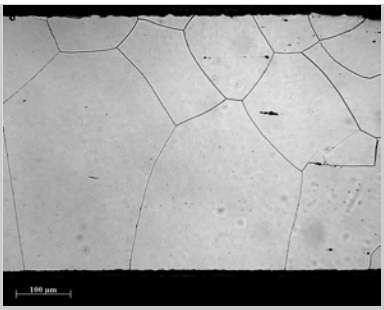	202,15	21,13	2,73	0,05

Table 12 *Data obtained for Steel C*

Sample	Microstructure	Main diameter (µm)	Standard deviation	P15/50 (W/Kg)	Standard deviation
I1000	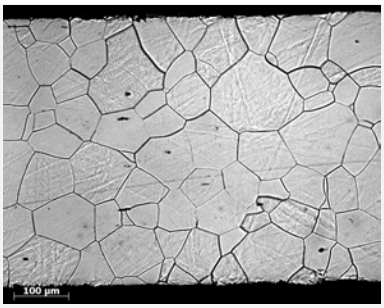	75,0	7,1	2,67	0,05
I1010	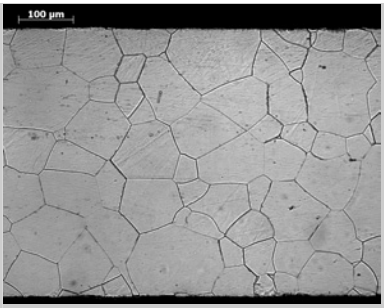	74,4	8,1	2,62	0,05
I1020		75,6	8,5	2,67	0,02
I1040	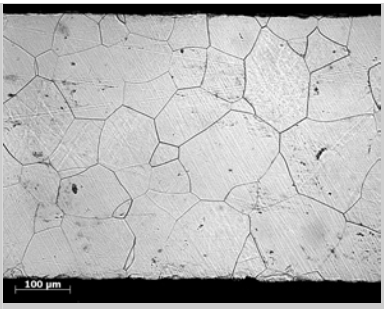	85,2	14,1	2,63	0,03
I1050	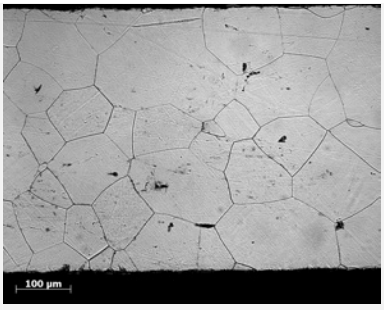	87,1	8,6	2,62	0,06

I1060		96,4	9,5	2,61	0,02
I1080		99,4	10,3	2,60	0,03
I1100		189,7	36,7	3,09	0,05

Table 13 *Data obtained for Steel D*

8 Summary

The influence of chemistry and soaking temperature (maximal temperature of the continuous annealing) on the final properties of non-oriented electrical steels has been studied. With this objective two different studies have been performed. First the Mn, Ni and Cr content of a low loss electrical steel composition has been modified. An intermediate content and a high content of each element has been added in order to study the influence of this components on the magnetic looses, grain size and texture. Secondly the influence of the soaking temperature on magnetic properties, grain size and oxidation in four grades of non-oriented electrical steels (Steel A, B, C and D) was studied.

Name: Ana Rodriguez Alonso

Date: 12/09/2008

Signature: